nature reviews materials

https://doi.org/10.1038/s41578-022-00506-0

Review article

Check for updates

Reactions in single-molecule junctions

Hongliang Chen [1,2,3] ✉, Chuancheng Jia[4,5], Xin Zhu[4,5], Chen Yang[5], Xuefeng Guo [4,5] ✉ & J. Fraser Stoddart [1,2,3,6] ✉

Abstract

Developing new materials is a long-standing goal that extends across the fields of synthesis, catalysis, nanotechnology and materials science. Transforming one compound or material into another involves the gaining, losing and sharing of electrons at a molecular level. Investigating single-molecule reactions — and understanding how they provide information about or differ from reactions in the bulk — will deepen our understanding of chemical reactions and establish new frameworks in materials science. In this Review, we survey state-of-the-art chemical reactions occurring in single-molecule junctions. We explore the advantages of real-time testbeds that deliver detailed information about reaction dynamics, intermediates, transition states and solvent effects. We provide a quantitative perspective of the charge transport phenomena associated with chemical reactions at molecular tunnelling junctions, and we compare the behaviour of single-molecule reactions and those taking place in ensemble states. Finally, we explore the possibility of leveraging single-molecule catalysis for large-scale production of materials.

Sections

[1]Stoddart Institute of Molecular Science, Department of Chemistry, Zhejiang University, Hangzhou, China. [2]Department of Chemistry, Northwestern University, Evanston, IL, USA. [3]ZJU-Hangzhou Global Scientific and Technological Innovation Center, Hangzhou, China. [4]Center of Single-Molecule Sciences, Institute of Modern Optics, Frontiers Science Center for New Organic Matter, College of Electronic Information and Optical Engineering, Nankai University, Tianjin, China. [5]Beijing National Laboratory for Molecular Sciences, National Biomedical Imaging Center, College of Chemistry and Molecular Engineering, Peking University, Beijing, China. [6]School of Chemistry, University of New South Wales, Sydney, New South Wales, Australia. ✉e-mail: hongliang.chen@zju.edu.cn; guoxf@pku.edu.cn; stoddart@northwestern.edu

Introduction

Chemical reactions typically involve changes in the positions of electrons as bonds break and form between atoms. Controlling the movement of electrons within or between molecules using different sources of energy — including heat, light, force, electrons and electric fields — enables the creation of a wide variety of products. To comprehend elementary chemical reactions, design catalysts and create new materials, it is essential to identify exactly how electrons participate in these transformations. In macroscopic experiments, however, the nuances of reaction mechanisms can be hidden for the simple reason that ensembles often display quasi-equilibrium conditions. Investigations of individual molecules can uncover[1–7] this hidden information, providing a more complete understanding of the mechanisms. Single-molecule techniques are beginning to occupy centre stage in the development of contemporary chemistry[8,9], such as in click chemistry[3], electric field catalysis[10,11], electrocatalysis[1], fluid catalytic cracking[2], nanoparticle catalysis[5], photo-induced reactions[12] and surface reactions[4]. In particular, the unique capabilities of molecular tunnelling junctions can provide fresh insights into photocatalysis[13], electrocatalysis[14], and other electron-transfer reactions[15] that involve electron transport.

A single-molecule junction (SMJ) consists of a conductive molecular bridge connected to two electrodes, one at each end. Reactions in SMJ platforms are performed by immobilizing the reactant or catalyst between electrodes. These reactions are initiated by applying external stimuli under different conditions. There are several advantages to studying chemical reactions in SMJs. Scanning tunnelling microscope (STM)-based or graphene-based SMJ techniques have demonstrated excellent compatibility with a variety of working conditions — from ambient conditions to ultrahigh vacuum at cryogenic temperatures, and even in liquid phases — a feature that enables extensive environmental control of single-molecule reactions. SMJ platforms enable reaction mechanisms to be investigated without the need for labels, by using electrical signals to probe reaction intermediates and/or transition states with high temporal resolution. They also have innate advantages beyond simply matching the size of the testbed to that of the single molecule being measured. The metal electrodes themselves can induce and affect reactions (Fig. 1a). It is not difficult to apply external stimuli to the junction to induce reactions trigged by light, chemicals, mechanical force (Fig. 1b), electrons (Fig. 1c) or electric fields (Fig. 1d). These stimuli, which can control the reactivity and selectivity of chemical reactions, have promoted the rapid development of the field of reactions in SMJs. Finally, investigating the role of solvents in single-molecule reactions helps to establish a catalytic model that is closer to homogeneous catalysis and to bridge the gap between single-molecule catalysis and reactions in the bulk. After these early discoveries, SMJ electrical testbeds have been developed continuously in order to achieve a balance between precision, controllability, reliability and scalability — and to further reduce the gap between single-molecule transformations and bulk reactions.

In this Review, we discuss how combining the art of synthetic chemistry with the practice of molecular electronics[16–23] can isolate single-molecule chemical reactions and monitor[24–27] their charge transport processes, revealing the chronology of reaction processes and encouraging the discovery of new phenomena of relevance to chemistry and materials science. We survey the capabilities of real-time SMJ platforms and the technical challenges that still need to be addressed. We also summarize the quantitative data analysis methods and machine-learning techniques developed to characterize single-molecule reaction kinetics and dynamics. Because the focal point of this Review is the application of single-molecule techniques towards synthetic chemistry, electrode-induced interfacial reactions (Fig. 1a), as usually used to form robust molecular circuits[28–33], are not emphasized here. We pay special attention to three reaction scenarios at SMJs: environmentally induced reactions (Fig. 1b), electron catalysis (Fig. 1c) and electric field catalysis (Fig. 1d). We believe that careful investigation of these single-molecule reactions will help to bridge the gaps between synthetic chemistry, heterogeneous catalysis and molecular electronics.

Stoichiometric analysis

Technical methods to probe single-molecule reaction kinetics and dynamics

The kinetics and thermodynamics of chemical reactions and catalyses have been investigated extensively using ensemble-averaged methods, such as in situ infrared spectroscopy[34], dynamic nuclear magnetic resonance spectroscopy[35], and transition absorption spectroscopy[36]. These techniques have also been used to gain real-time insight into continuous reaction trajectories. Probing chemical reactions with single-molecule precision (Box 1) can provide mechanistic insights into reaction kinetics[37,38] and catalytic dynamics[39,40], distinguish alternative reaction pathways[41,42], and even capture intermediate species[43] that are usually hidden within a distribution in the ensemble-averaged measurements. For single-molecule reactions in condensed phases — namely, in solution or on surfaces[44,45] — single-molecule fluorescence microscopy[2,8,37,45] and single-molecule Raman scattering spectroscopy[46–49] have been employed to reveal the reaction kinetics and/or dynamics associated with solvents and external stimuli. Single-molecule fluorescence microscopy, however, usually requires[4] the use of fluorescent labels. The diffusion of homogeneous reactions in solution makes it far from easy to capture fluorescent signals. Single-molecule Raman spectroscopy often suffers[48–50] from plasmonic effects and low signal intensity.

The SMJ platform provides a label-free tool for real-time probing of intermediates, transition states and reaction trajectories, which are transduced directly into electrical signals. We note that the statistical results for single-molecule reactions are obtained from continuous measurements on a single molecule instead of from observations of ensembles, and thus the single-molecule dynamic analyses are defined on the average within a time domain, which should be comparable to the macroscopic thermodynamic results based on ensemble average.

Kinetic and dynamic analysis methods for graphene SMJs

Beyond these advances in 'hardware' (Box 1), the development of 'software' (Fig. 2) — namely, data analysis methods — is also crucial to process the vast array of electrical signals associated with specific reaction states. For example, real-time electrical measurements of single-molecule nucleophilic additions (Fig. 2a), based on graphene SMJs, produce[51] a large amount of reproducible current fluctuations between two states (Fig. 2b, step 1) that can be transduced into a rich supply of molecular structural signatures associated with intermediates in chemical reactions. Kinetic and dynamic analysis methods are employed to treat these stochastic data (Box 2). First, one-dimensional histogram analyses of current values are performed in order to achieve a bimodal current distribution (Fig. 2b, step 2). These two distinct states can be attributed to the reversible transformation between a reactant and an intermediate. Second, by using the QuB software[52], the current–time curves can be fitted with two distinguishable states using a segmental *k*-means method based on hidden Markov model analysis (Fig. 2b, step 3). Dwell times (τ_{high} or τ_{low}) for the high- and low-conductance states, respectively, can therefore be obtained from the ideally fitted

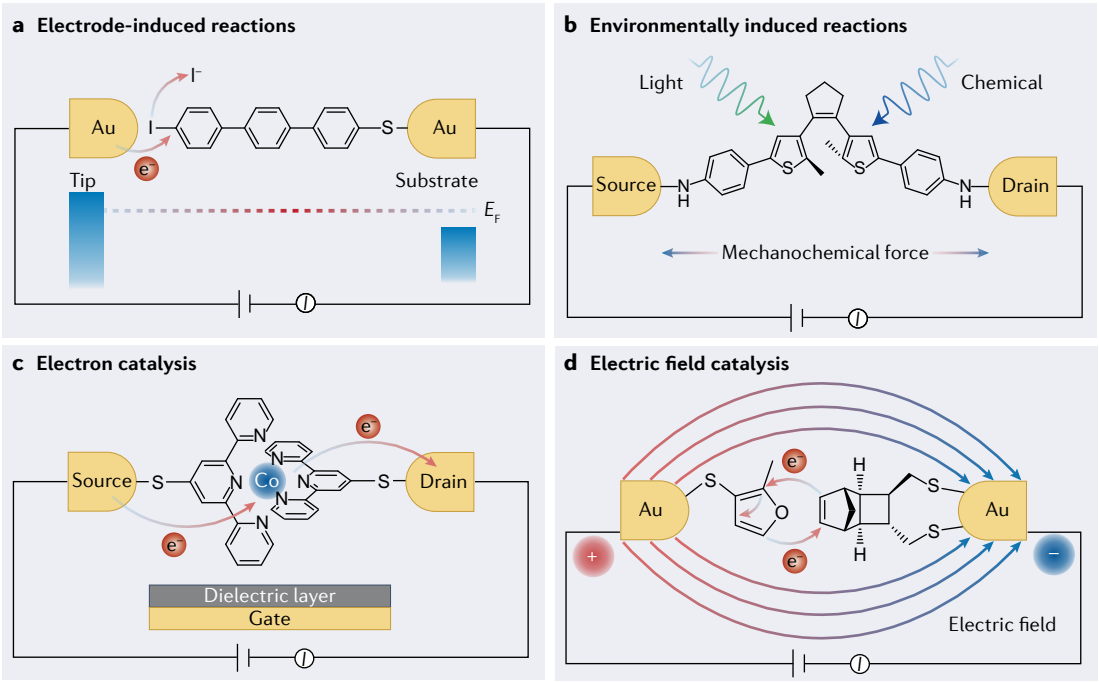

Fig. 1 | Four reaction scenarios in single-molecule junctions. a, Electrode-induced reactions. In an electrode-induced reaction, an Au–C bond is formed in order to realize robust contacts between the molecule and the electrodes. **b**, Environmentally induced reactions. The external stimuli used to induce these reactions include chemicals, mechanical force, light and plasmon. **c**, Electron catalysis. In electron-mediated reactions, electrons undergo exchange between electrodes and molecules. **d**, Electric field catalysis. Large external electric fields are applied over small distances between two electrodes in order to induce reactions. Panel **a** adapted with permission from ref.[31], copyright 2020 American Chemical Society. Panel **b** adapted with permission from ref.[112], AAAS. Panel **c** adapted from ref.[143], Springer Nature Limited. Panel **d** adapted from ref.[20], Springer Nature Limited.

current–time curves. Third, by plotting and fitting the dwell times of each state using a single-exponential function, the average lifetime of the corresponding states can finally be achieved (Fig. 2b, step 4). These average lifetimes can then be used[53] to calculate the reaction kinetic and dynamic parameters, such as the activation energy (E_a) and the equilibrium constant (K). This methodology determines the lifetime of intermediate states and the kinetic and dynamic parameters in each key step of a chemical reaction. We note that the parameters obtained from statistical analysis of single-molecule current–time curves are compatible[51,53–56] with the theoretical calculations, proving the reliability of the quantification of the reaction rates and energy barriers.

Kinetic analysis methods for break-junction techniques

Break-junction measurements consist of repeatedly forming a point contact with a single molecule while simultaneously measuring the conductance as a function of the tip–substrate displacement. Each breaking trace provides[57,58] information about the constitution of the molecule – either a reactant, an intermediate or a product – in the junction. The kinetics of chemical reactions at the single-molecule scale can be extracted[59–61] quantitatively by determining the distributions of conductance[61] (Fig. 2c) or the displacement[62] (Fig. 2d). Time-dependent peak area ratios of reactants, intermediates and products can be obtained by multiple-peak Gaussian fitting. Therefore, the percentage of products in all molecular junctions with respect to time can be determined and employed in further kinetic analysis. In addition, flicker noise analysis (Fig. 2e) can be used[63] to investigate conformational interconversion processes.

The application of machine-learning algorithms[64] (Fig. 2f) to break-junction techniques is another important advance in data-analysis methods that has occurred during the past 5 years. The conventional analysis (Fig. 2f, top left) of breaking traces involves creating one- and two-dimensional conductance histograms from all the measured traces and obtaining an average junction conductance of reactants, intermediates and products. Machine-learning tools[65] can tackle the problem by extracting and analysing multiple aspects of measured data, classifying different breaking traces, and distinguishing electrical signals from reactants, intermediates and products. First, a breaking trace (Fig. 2f, step 1) is converted into an individual two-dimensional feature vector (Fig. 2f, step 2). Second, an appropriate machine-learning algorithm[65–70] (Fig. 2f, step 3) is chosen to categorize the data into different clusters (Fig. 2f, step 4). Finally, the clusters can be used to reconstruct one-dimensional histograms belonging to different chemical species (Fig. 2f, step 5). In a further step, automated methods based on machine learning can be employed[71–73] to detect and optimize reaction conditions autonomously at SMJs with high throughput. When used together with quantum chemical calculations, machine-learning approaches can also provide an understanding of chemical reactivities[74–76] in single-molecule reactions.

Capturing reaction intermediates from real-time data

Mechanistic analysis from ensemble experiments can outline a catalytic cycle by presenting some node information, such as the capture of reaction intermediates. The catalytic cycle is divided into several independent steps according to the elementary reaction under investigation.

Box 1

Single-molecule reaction probing platforms

Optical platforms

Optical methods are employed to investigate chemical reactions taking place in condensed phases in order to reveal molecular reaction kinetics and/or dynamics associated with solvents and external stimuli. Single-molecule fluorescence microscopy[219] (see table and panel **a** of the figure) and single-molecule Raman scattering spectroscopy[220] (see table and panel **b** of the figure) have emerged as tools with which to investigate reaction mechanisms, by providing fluorescent signals[8] and vibrational signatures[164] of the bond transformations, respectively.

Imaging platforms

Surface imaging techniques for chemical reactions provide in situ initiation[221–223] and direct visualization[214,224] of chemical bond transformations on surfaces[225] with single-atom and even single-bond precision. An ultrahigh-vacuum scanning tunnelling microscope[226] (STM) (see table and panel **c** of the figure) and non-contact atomic force microscope[214] (AFM) (see table and panel **d** of the figure) with ultrahigh vacuum, ultralow temperature and ultraclean crystalline metallic surfaces are often used in these investigations.

Junction platforms

Junction platforms are applied to chemical reactions in which the reactants or catalysts are immobilized between electrodes. STM break-junction[20,23] (see table and panel **e** of the figure) and graphene single-molecule junction (see table and panel **f** of the figure) techniques[51,53], which are highly compatible in a variety of working conditions, have been developed in recent years to achieve a balance between precision, controllability, reliability and scalability.

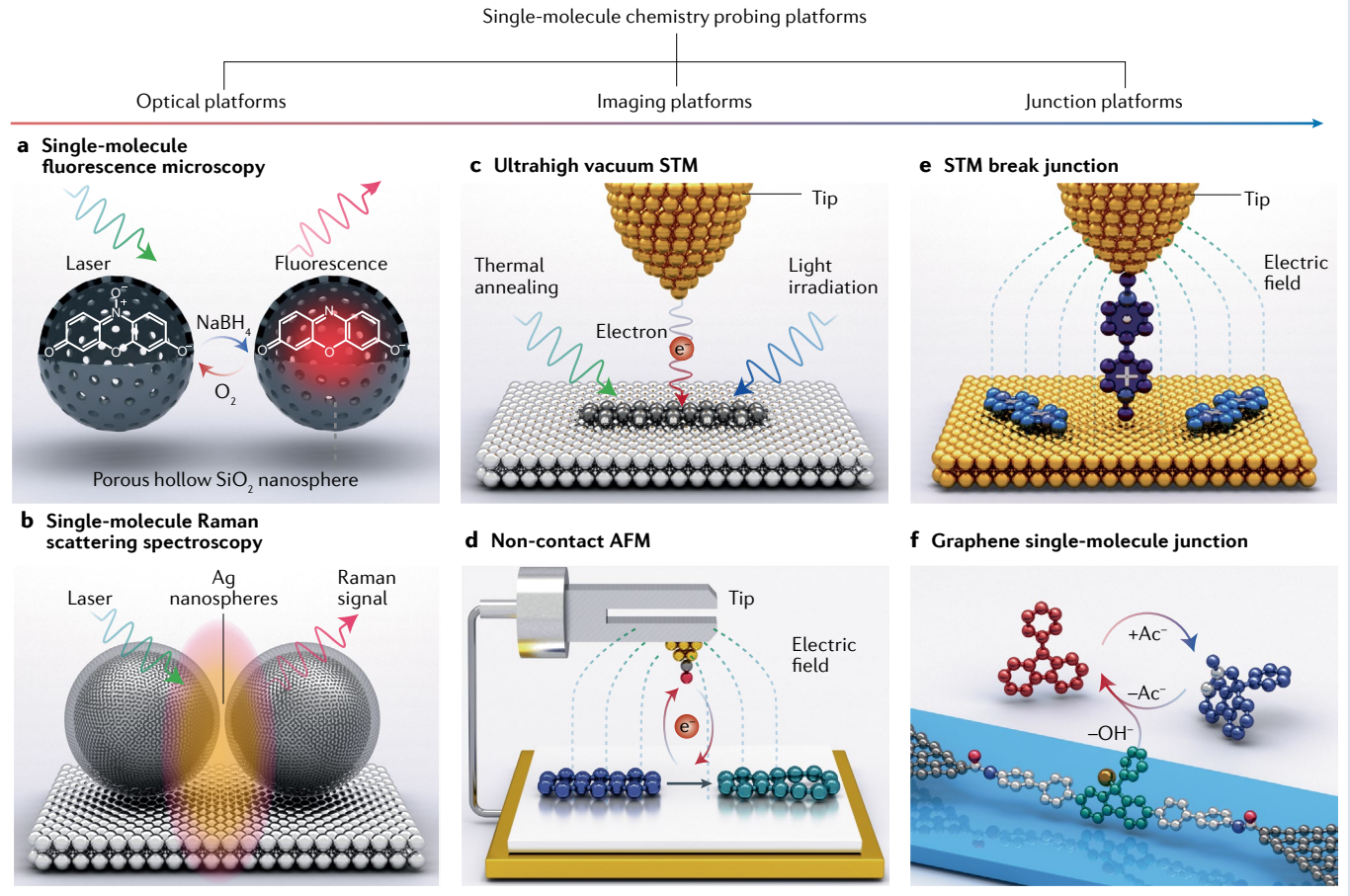

Panel **f** of the figure adapted with permission from ref.[53], copyright 2018 American Chemical Society.

(continued from previous page)

Platform	Advantages	Disadvantages
Single-molecule fluorescence microscopy	Robust reaction conditions; multiple environmental control methods; reactions are performed in solutions or on surfaces under ambient conditions	Requires fluorophore labelling; photobleaching; thermal effects; diffusion of molecules in solution
Single-molecule Raman scattering spectroscopy	Multiple environmental control methods; provides vibrational signatures of chemical bonds	Low signal intensity; requires plasmonic nanocavity substrate; plasmonic effects
Ultrahigh-vacuum STM	Reactions are triggered by thermal annealing, light irradiation, tunnelling electrons or electric fields; direct visualization of chemical reactions; imaging capability with molecular and atomic-scale precision	Harsh operation conditions (ultrahigh vacuum, ultralow temperature and ultraclean crystalline metallic surface); requires rational design of starting materials
Non-contact AFM	Injecting electrons; tip manipulation; imaging capability with single-bond and single-atom resolution	Harsh operation conditions (ultrahigh vacuum, ultralow temperature and ultraclean crystalline metallic surface); limited reaction scope
STM break junction	High compatibility under different working conditions; applying electric fields and injecting electrons	No imaging capability; relatively poor reaction kinetics/dynamics analysis capability
Graphene single-molecule junction	Multiple external control methods; applying electric fields and injecting electrons; integrating with other techniques; real-time measurement of currents; long junction lifetimes; high stability; detection of reactive intermediates; quantitative analysis of reaction kinetics/dynamics	No imaging capability; heavy data-processing tasks; sophisticated nanofabrication process

These steps provide static, indirect and partial information of the reaction trajectory. A complete picture of the catalytic cycle can be obtained by splicing this node information. Using the SMJ technique to investigate reaction mechanisms is based on the analysis of real-time current data from the molecular wire, which is undergoing chemical transformation. The SMJ technique can track the catalytic cycle of a focused single catalyst (Fig. 3a) in situ and in real time[56], producing a dynamic, intuitive and comprehensive image of the full cycle (Fig. 3b,c).

For example, the distinction between the two controversial pathways in the widely investigated Suzuki–Miyaura cross-coupling (Fig. 3d) can be addressed by monitoring[56] this catalytic cycle in a single-catalyst junction. Starting with the oxidative addition complex **2**, the first proposed pathway (Fig. 3d, solid arrows) exchanges the ligand with the base before interacting with boronic acid, leading to the intermediate **4**. In the second pathway (Fig. 3d, dashed arrow), complex **2** reacts directly with the base-activated boronic acid complex **6** to produce intermediate **4**. The reaction involves the same species in both mechanisms, hampering clarification of the pathways in ensemble experiments.

Monitoring the current travelling through a single catalyst integrated in electrodes (Fig. 3a), however, addresses this conundrum. The periodic electrical signal (Fig. 3b), which includes four main conductance states (Fig. 3c), reflects the catalytic cycle of the Suzuki–Miyaura coupling reaction. These conductance states are assigned to each intermediate in the cycle through a series of control experiments, inelastic electron tunnelling spectroscopy, and intermediate-limited experiments combined with theoretical simulations (Fig. 3d). The time sequence of the detected species supports a transition from complex **3** to intermediate **4**, providing direct evidence that the ligand-exchange pathway is dominant in the Suzuki–Miyaura coupling reaction mechanism.

In contrast with ensemble experiments in solution, the thermodynamic and kinetic parameters of each elementary reaction step of the single-molecule cross-coupling can be extracted simultaneously by statistical analysis (Fig. 3e). The rate constants for oxidative addition and ligand exchange (**1**→**3**, ~361.7 s^{-1}), pre-transmetallation (**3**→**4**, ~214.7 s^{-1}), transmetallation (**4**→**5**, rate-determining step, ~178.4 s^{-1}) and reductive elimination (**5**→**1**, ~238.8 s^{-1}) demonstrate the intrinsic kinetics characteristics of the Suzuki–Miyaura cross-coupling. Furthermore, the conversion rates between complex **1** and **4** can also be estimated. The low k_{14} ($5.9 \pm 0.3\ s^{-1}$) and k_{41} ($2.7 \pm 1.0 \times 10^{-4}\ s^{-1}$) indicate that there is no direct reaction between complex **2** and **6** to give intermediate **4**, and clarifies the reaction mechanism from a kinetic perspective. The unique ability of SMJ techniques to detect intermediate species and their time sequences[54] provides powerful capabilities for deciphering mechanisms, opening up ways to reveal reaction processes and guiding macroscopic organic syntheses.

Environmentally induced reactions

The earliest chemical reactions studied in SMJs fell under the umbrella of molecular switching[77]. In a single-molecule circuit, switching is based on an intrinsic bi-stable change of the internal structure[12] — for example, a constitutional change[78] or a configurational change[79] in a single-molecule reaction — which induces a modification in the conductance. The variations in conductance can be utilized to determine the switching mechanism of the molecule. The molecular switching can be facilitated by external stimuli[80] of macroscopic origin, such as chemicals (reactants, pH, solvents), or mechanical forces, or light, or by plasmons in nanogaps[81] for control on the mesoscopic scale.

Chemically induced reactions

Chemically induced single-molecule reactions can be dated back to the application of [2]catenanes[82] and [2]rotaxanes[83] as molecular switches, which undergo co-conformational changes upon chemical or electrochemical induction (Fig. 4a). In these mechanically interlocked molecules, a ring moves around a second ring or along the axle of a dumbbell and occupies one of two recognition sites, one of which provides a high-conductance state and the other a low-conductance state. The union of mechanically interlocked molecules with molecular electronics[17,84–86] has enabled mechanical bonds to be understood on a molecular level[87] from both mechanical and electrical perspectives. Some proof-of-concept experiments, performed using a graphene SMJ platform, have demonstrated[88,89] the dynamic switching of a single (pseudo)rotaxane undergoing a shuttling-like motion in aqueous solution. Other chemically induced single-molecule reactions, such

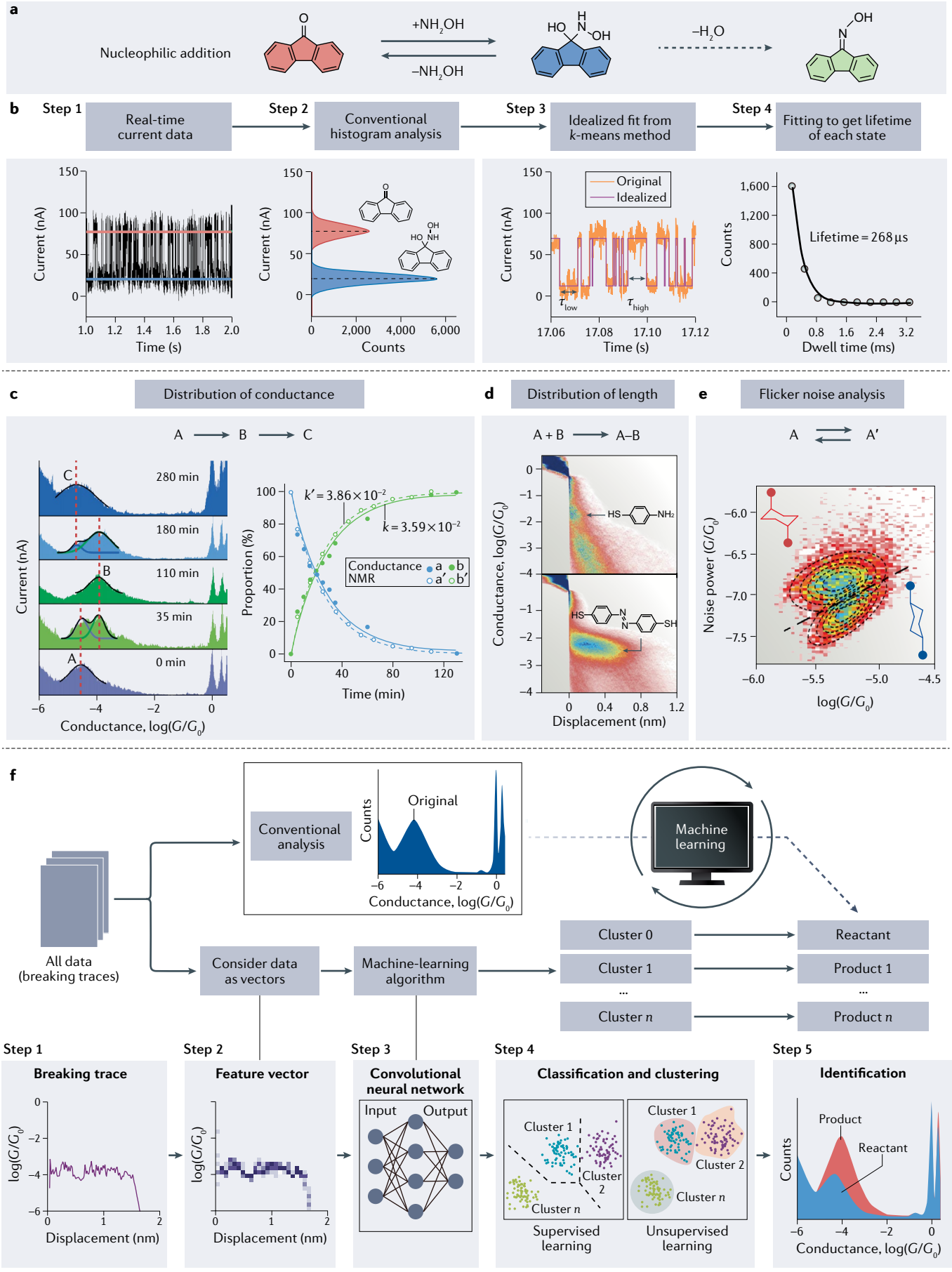
a
Nucleophilic addition
+NH2OH
–NH2OH
–H2O
b
Step 1
Real-time current data
Step 2
Conventional histogram analysis
Step 3
Idealized fit from k-means method
Step 4
Fitting to get lifetime of each state
Current (nA)
Time (s)
Counts
Original
Idealized
Lifetime = 268 µs
Dwell time (ms)
c
Distribution of conductance
A → B → C
280 min
180 min
110 min
35 min
0 min
Conductance, log(G/G0)
k′ = 3.86×10−2
k = 3.59×10−2
Conductance a a′ b b′
NMR
Proportion (%)
Time (min)
d
Distribution of length
A + B → A–B
Conductance, log(G/G0)
Displacement (nm)
e
Flicker noise analysis
A A′
Noise power (G/G0)
log(G/G0)
f
All data (breaking traces)
Conventional analysis
Original
Machine learning
Consider data as vectors
Machine-learning algorithm
Cluster 0
Cluster 1
Cluster n
Reactant
Product 1
Product n
Step 1
Breaking trace
Displacement (nm)
Step 2
Feature vector
Step 3
Convolutional neural network
Input
Output
Step 4
Classification and clustering
Supervised learning
Unsupervised learning
Step 5
Identification
Product
Reactant

Fig. 2 | Real-time data-analysis methods. a, A single-molecule nucleophilic addition. **b**, Illustration of current–time data analysis for extracting the kinetic parameters of single-molecule reactions. Step 1: real-time electrical data showing the current fluctuations between two states. Step 2: one-dimensional histogram analyses of the real-time current data, demonstrating a bimodal current distribution. Step 3: theoretical fit of the current–time curves with two distinguishable states using a segmental *k*-means method. Step 4: average lifetime of the low-conductance state achieved by plotting and fitting the dwell times in step 3. **c**–**e**, Illustration of stoichiometric analysis for reactions in break junctions. **c**, Monitoring the transformation from A to B to C by analysing the distribution of conductance. The histograms are analysed by Gaussian fitting to determine the area ratio between different components. Right inset: comparison of reaction kinetics for the reaction A to B in a single-molecule junction and in an nuclear magnetic resonance (NMR) tube. A, reactant; B, intermediate; C, product. **d**, Monitoring the coupling between A and B by analysing the distribution of molecular junction lengths. A, reactant; B, reactant; A–B, the coupling product. **e**, Monitoring the transition between two stable conformations of a molecule using flicker noise signals. A, conformation 1; A′, conformation 2. **f**, Illustration of using machine-learning methods for data analysis. Step 1: one example of a breaking trace obtained from break-junction measurements. Step 2: transformation of a breaking trace into a feature vector. Step 3: machine-learning algorithms chosen to classify the created feature space. Step 4: classification and clustering results obtained for the database of all breaking traces. Step 5: identification of different chemical species by reconstructing the conductance histograms from different clusters. Panels **a** and **b** reprinted with permission of AAAS from ref.[51], © The Authors, some rights reserved; exclusive licensee AAAS. Distributed under a CC BY-NC 4.0 License (http://creativecommons.org/licenses/by-nc/4.0/). Panel **c** adapted with permission of AAAS from ref.[61]. © The Authors, some rights reserved; exclusive licensee AAAS. Distributed under a CC BY-NC 4.0 License (http://creativecommons.org/licenses/by-nc/4.0/). Panel **d** adapted with permission from ref.[62], copyright Wiley-VCH GmbH, and adapted from ref.[217], Springer Nature Limited. Panel **e** adapted with permission from ref.[63], Elsevier. Panel **f** adapted from ref.[68], CC BY 4.0 (https://creativecommons.org/licenses/by/4.0/).

as the reversible protonation and deprotonation of molecular junctions[90–92], focus on harnessing the chemical and electronic structural changes in molecules before and after a reaction in an attempt to build molecular switches.

The mechanisms of chemically induced transformations have only occasionally been the focus of molecular electronics. The key to bridging the gap between current signals and reaction mechanisms is the use of real-time single-molecule testbeds. By monitoring the change in current as a function of time with high temporal resolution, the reaction kinetics can be determined. For example, graphene SMJ platforms can be applied to probe the dynamic details of nucleophilic substitutions[53] and additions[51]. The activation energy ($E_c \approx 50$ kJ mol^{-1}) of a single-molecule nucleophilic substitution, a value comparable to the macroscopic results (~42 kJ mol^{-1}), can be derived from the real-time current signals. The dynamics and solvent dependence of a reversible nucleophilic addition can be measured by changing the solvents in the SMJ platform[51]. These investigations have revealed ways[27] to probe intermediates directly with high temporal resolution in not only single-molecule chemical reactions but also in single-molecule reactions involving both proteins[93,94] and DNAs[95,96], broadening the contribution of SMJ platforms to fields beyond reaction mechanisms in chemistry.

Mechanochemical force-induced reactions

Mechanical force is an important way to induce transformations of molecular wires, especially during break-junction measurements. There are three known mechanisms associated with force-induced single-molecule reactions. First, mechanical distortion in a molecule with a redox centre can induce electron-transfer reactions[97,98] by creating a favourable nuclear geometry that allows electron transfer to take place (Fig. 4b). For example, mechanical stretching of coordinative metal–ligand bonds is responsible for shifts in energy levels and redox potentials[99]. Mechanical pulling may also distort[100] the Fe(II) coordination sphere and eventually modify its spin states (Fig. 4c, top). Second, in permethyloligosilane molecules[101], force can induce conformational changes – without bond rupture – between three distinct conformations with dramatically different electronic properties. The nuanced conformational changes are associated with a stereoelectronic effect. By simply stretching or compressing the molecular oligosilane junctions, conductance can be switched digitally between the three conformations. Third, force can trigger[102] the isomerization[103,104] of a ring-closed spiropyran to its zwitterionic merocyanine ring-opened state (Fig. 4c, bottom). Physically pulling the ends of the molecule breaks the spiro C–O bond, causing a large change in electronic conjugation, as indicated by colour changes in the bulk state and dramatic conductance variations at the single-molecule level.

For most of these force-induced single-molecule reactions, however, theoretical calculations are needed to elucidate the interplay between the electronic properties and structural variations of the molecules. In future, more reliable experimental results can be expected from combining[105,106] break-junction measurements with single-molecule force spectroscopy, thus improving our understanding of the connection between force and conductance during chemical bond dissociation and formation.

Photo-induced reactions

Light is a clean, non-invasive and easily addressable way to trigger[107,108] switches in photochromic molecules (Fig. 4d). SMJs provide an effective real-time in situ platform with which to monitor[12] photochemical processes that are relevant to chemical and biological systems. Investigations of reversible photo-isomerizations at the single-molecule level, however, remain challenging.

A photochemical reaction usually involves a photo-excited state. When performing photochemical reactions in single-molecule devices, the photo-excited state is often quenched by the electrodes, affecting the reversibility of the intrinsic photochemical process. This quenching phenomenon is caused mainly by two factors: the relative position between the Fermi level of the electrodes and the energy level of the excited molecule[109], and/or electronic coupling between the electrodes and the molecule at the interface[110]. For example, a diarylethene molecule is typically photochemically reversible between high-conductance (closed) and low-conductance (open) states, but it loses this reversibility when connected to nanogap gold electrodes in a single-molecule device (Fig. 4e). This loss occurs because the Fermi level of gold is close to the energy level of the excited state of the diarylethene molecule in its open form, quenching this excited state and inhibiting the molecule from returning to the closed form[109,111] (Fig. 4f). By contrast, when diarylethene is connected to carbon nanotube electrodes (Fig. 4g), strong interface coupling between the molecule and electrodes quenches the photo-excited state of the closed form, such that the molecule cannot return to the open form[110] (Fig. 4h). These results highlight the importance of the molecule–electrode contact interface to the device function.

The challenge of molecular excited state quenching can be solved by molecular engineering to tune the energy level alignment and electronic coupling at the molecule–electrode interface. A hydrogenated diarylethene derivative with electron-donating properties has higher energy levels than the pristine molecule, whereas the fluorinated derivative, with all its electron-withdrawing fluorine atoms, has lowered energy levels[112–114]. To control the electronic conjugation at the interface and weaken interface coupling, saturated oligomethylene chains with one to three methylene groups can be introduced as

Box 2

Kinetic and dynamic analysis of single-molecule reactions

The quantitative kinetic and dynamic parameters of a single-molecule reaction can be extrapolated from real-time current–time plots (Fig. 2b). The time interval between two current states is called the dwell time (τ) of one state, which is afforded by idealizing current–time trajectories using[52] the QuB software. The distributions of the dwell time are fitted in a single exponential decay function:

$$P(\tau) = \frac{1}{\langle\tau\rangle}\exp\left(-\frac{\tau}{\langle\tau\rangle}\right) \quad (1)$$

where $\langle\tau\rangle$ is the mean duration time. Other kinetic and dynamic parameters can be determined from $\langle\tau\rangle$. First, the kinetic constant k_T is the reciprocal of $\langle\tau\rangle$, and then the activation energy E_a of each process is obtained through the linear fitting of $\ln k_T$ with respect to $1/T$ according to the Arrhenius equation:

$$k_T = A(T)\exp\left(\frac{-E_a}{RT}\right) \quad (2)$$

where $A(T)$ is the pre-exponential factor, R is 8.314 J mol^{-1} K^{-1} and T is the temperature.

Second, the energy difference ΔE between two states is obtained according to Boltzmann statistics[227,228]:

$$\Delta E = -RT\ \ln\frac{\langle\tau_1\rangle}{\langle\tau_2\rangle} \quad (3)$$

Third, the Gibbs free energy[229], ΔG, can be derived from:

$$\Delta G^0 = -RT\ \ln K^0 \quad (4)$$

The equilibrium constant K^0 should be redefined in single-molecule reactions. In the case of first-order reactions, ΔG is equal to the energy difference ΔE of two states, leading to an equilibrium constant $K^0 = k_1/k_2$. In second-order reactions, however, an extra correction is required on account of the dispersed reactant concentrations. In this situation, the equivalent equilibrium constant K is corrected using the Langmuir isotherm model:

$$K = \frac{\alpha}{1-\alpha}C \quad (5)$$

where α represents the proportion of one of the stable states of the immobilized single molecule in the junction, and C is the concentration of other interacting molecules dispersed in the solution[230]. Enthalpy (ΔH) and entropy (ΔS) for the two stable states of the single-molecule reaction can also be determined from:

$$\Delta G = \Delta H - T\Delta S \quad (6)$$

which is similar to the thermodynamic equation employed in macroscopic reactions in solution. Last, when the transition-state theory is introduced, the $\Delta H^{\neq}$ and $\Delta S^{\neq}$ between the transition state and substrate can be determined from the van't Hoff equation:

$$R\ \ln\frac{h}{\langle\tau_1\rangle k_B T} = -\frac{\Delta H^{\neq}}{T} + \Delta S^{\neq} \quad (7)$$

According to the quantitative analysis of single-molecule reaction dynamics, the information hidden in the averages of macroscopic reactions in solution can be obtained from the observation of single events in single-molecule junctions.

linkers on both sides of the diarylethene centre (Fig. 4i). In the case of a hydrogenated diarylethene derivative with two trismethylene linkers[112], these modifications led to a fully reversible light-controlled change in single-molecule conductance between the high- and low-conductance states (Fig. 4j). This observation proves that intrinsic photochemical processes involving single molecules can be monitored successfully in specially designed single-molecule devices.

Photo-isomerizations that take place in SMJ platforms are more complicated than those in solution because tunnelling electrons, electric fields and external light irradiation all contribute to the switching. Disentanglement of these contributions is not an easy task. For example, a single molecule of azobenzene is known to undergo reversible *cis*-to-*trans* isomerization induced by light[115,116], by tunnelling electrons[117,118] and by electric fields[21,119,120]. In another case, a bicyclic norbornadiene can switch to the quadricyclane form upon illumination by UV light and relax thermally to the original state[121]. When located in an SMJ, however, the norbornadiene-to-quadricyclane isomerization is activated thermally by local heating, whereas the reverse transformation is realized by a single-electron-transfer process using a high bias. Elegant control experiments need to be designed to understand the mechanisms that contribute to each direction of a reversible photo-isomerization. Figuring out the role of reaction conditions in controlling the switching direction may realize multiple controllable modes of inducing isomerization beyond the use of light, while providing unique alternative approaches, such as tunnelling electrons, electric fields and local heat, for investigating the mechanisms of isomerization at both the atomic[122] and molecular[123] levels.

Plasmon-induced reactions

The external stimuli used to facilitate the above chemical transformations have macroscopic origins. Plasmons in nanogaps may provide[81,124] a more controlled means of manipulating single-molecule reactions on the mesoscopic scale. In general, plasmon-mediated reactions[48–50] can be invoked by four excitation mechanisms[124]: a direct intramolecular excitation, an indirect hot-electron transfer, a charge transfer from metal to molecules, or local heating involving vibrational excitation of molecules. Which excitation mechanisms are associated with a given reaction remains controversial because hot carriers, strong electric fields and photothermal effects can all contribute[125,126] to the transformation and are difficult to disentangle.

The STM platform — by revealing the identity of the substrate, exercising accurate temperature control, performing light energy and intensity dependence measurements and ensuring real-space single-molecule observations — can provide a fundamental understanding of the different excitation mechanisms in plasmon-induced reactions at the single-molecule level. For example, direct intramolecular excitation is found to be the principal mechanism in the plasmon-induced dissociation of dimethyl disulfide[124], for the simple reason that the molecule is hybridized weakly with the metal substrate. In the plasmon-induced dissociation of O_2, however, hot-carrier transfer is the dominant mechanism because O_2 is chemisorbed strongly on the silver substrate[127]. We note that molecular junctions are complex systems that cannot be elucidated fully using theoretical models of optical-electrical behaviour in biased junctions, which are always simplified to tackle plasmon-induced reaction mechanisms.

Electron catalysis

Electron catalysis is a key technology for realizing the transition of industrial synthesis from relying on fossil energy to employing renewable energy such as electricity. Investigating the role of electrons during

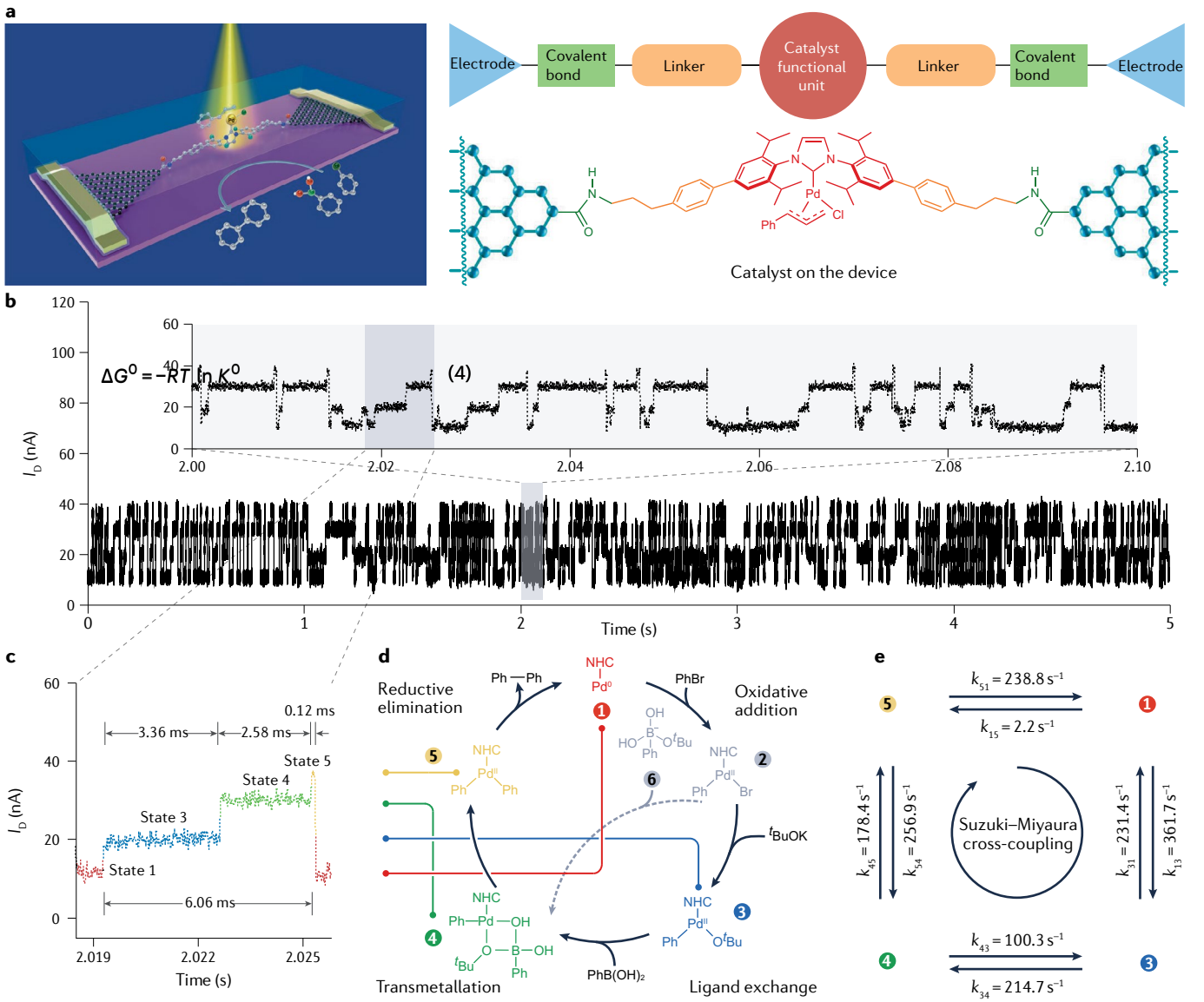

Fig. 3 | Revealing new reaction pathways from dynamic analysis of single-molecule reactions. a, Schematic illustration (left) and structural formula (right) of a single-molecule catalyst immobilized between graphene electrodes for real-time monitoring of a Suzuki reaction. **b**, Real-time detection of current changes for 5 s on account of the change of the decoupled catalytic function centre. Inset: current signal fluctuations between multiple states in an expanded region covering 100 ms. **c**, One stepwise catalytic cycle covering 6 ms demonstrating four different conductance states. **d**, A complete catalytic cycle of a Suzuki–Miyaura cross-coupling reaction showing two possible transmetallation pathways. One mechanism comprises ligand exchange of an oxidative addition complex **2** with a base to give **3**, which then interacts with a boronic acid leading to a transmetallation intermediate **4**. In the other mechanism, complex **2** undergoes transmetallation directly with the base-activated complex **6** to give the intermediate **4**. **e**, Extraction of the conversion rates between species **1**, **3**, **4** and **5** in the catalytic cycle. I_D, source–drain current; k, rate constants of reactions. Adapted from ref.[56], Springer Nature Limited.

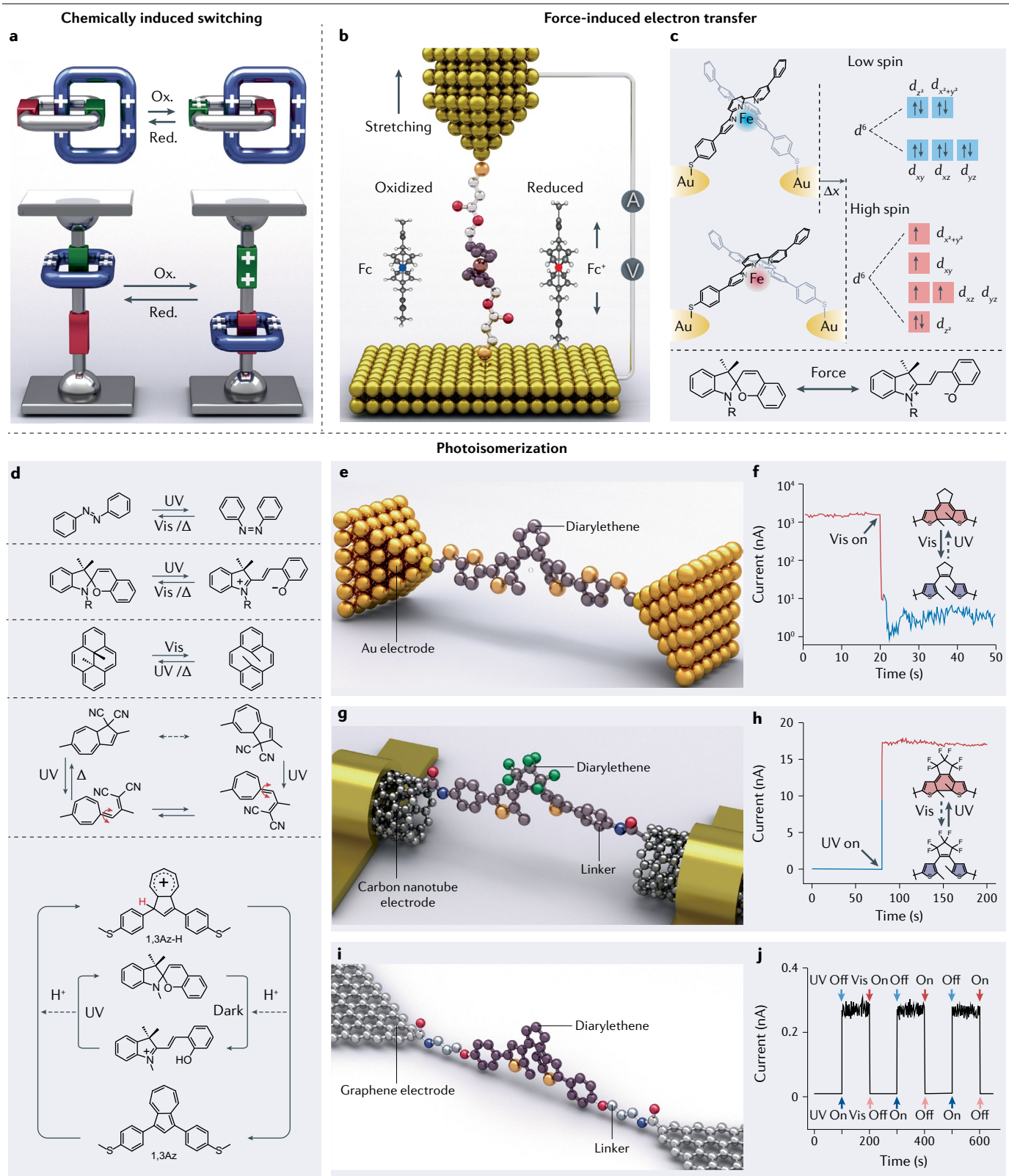
Chemically induced switching
Force-induced electron transfer
a
b
c
Ox.
Red.
Ox.
Red.
Stretching
Oxidized
Reduced
Fc
Fc+
A
V
Low spin
High spin
Fe
Au
Au
Δx
Force
Photoisomerization
d
e
f
UV
Vis /Δ
Vis
UV /Δ
Diarylethene
Au electrode
Vis on
Vis
UV
Current (nA)
Time (s)
g
h
Diarylethene
Linker
Carbon nanotube electrode
UV on
Vis
UV
Current (nA)
Time (s)
i
j
Diarylethene
Linker
Graphene electrode
UV Off Vis On Off On Off On
UV On Vis Off On Off On Off
Current (nA)
Time (s)
1,3Az-H
1,3Az
H+
UV
Dark
H+
HO

Fig. 4 | Environmentally induced reactions. a, Top: chemically induced switching of a bi-stable [2]catenane. Upon addition of an oxidant, the blue ring changes from encircling the green recognition site to encircling the red one. When a reductant is added, the blue ring returns from encircling the red site to encircling the green one. Bottom: chemically induced switching of a bi-stable [2] rotaxane. The ring moves along the axle of a dumbbell and occupies either the red or the green recognition site upon addition of an oxidant and a reductant, respectively. **b**, Schematic illustration showing a stretching-induced electron-transfer reaction in a ferrocene (Fc)-based single-molecule junction. As the ferrocene derivative is stretched by the movement of one electrode, it becomes oxidized. **c**, Top: a mechanically controlled single-molecule junction based on an Fe(II)-based spin-crossover molecule. Stretching of electrodes distorts the Fe(II) coordination sphere and changes the spin states. Bottom: force-induced isomerization of a spiropyran. Pulling the ends of the molecule breaks the spiro C–O bond. **d**, Single-molecule photo-isomerizations. **e**, A single-molecule photochromic diarylethene switch attached to two Au electrodes. **f**, Current–time plot showing irreversible switching of diarylethene in panel **e** from the closed to open state upon applying visible light. **g**, A photochromic diarylethene molecular junction connected to carbon nanotube electrodes. **h**, Current–time plot showing irreversible switching of diarylethene in panel **g** from the open to the closed state upon ultraviolet irradiation. **i**, A graphene-electrode-based single-molecule diarylethene junction in which the diarylethene switch has been extended by incorporating trismethylene linkers at each end of the switch. **j**, Current–time plot showing the reversible current of diarylethene in **i** switching through a diarylethene junction between its open and closed forms, upon ultraviolet (UV) and visible (Vis) light irradiation. Δ, heat. Panel **a** adapted from ref.[86], Springer Nature Limited, and adapted from ref.[218], Springer Nature Limited. Panel **b** adapted with permission from ref.[99], copyright 2017 American Chemical Society. Panel **c** (top) adapted with permission from ref.[100], copyright 2016 American Chemical Society. Panel **d** (bottom) adapted with permission from ref.[92], copyright Wiley-VCH GmbH. Panel **j** adapted with permission from ref.[112], AAAS.

molecular transformations is essential when it comes to understanding electrocatalysis at the macroscopic scale. The SMJ technique provides a versatile platform with which to investigate electron transport during a chemical reaction at the single-molecule level. To convert an SMJ platform into a toolkit for studying electrocatalytic mechanisms, the first issue to address is to establish the connection between the microscopic data recorded during single-electron-transfer reactions at SMJs and the macroscopic data obtained from electrochemical reactions in the bulk. We anticipate that comparative investigations of this kind will help to enable stochastic electron-catalysed single-molecule reactions using deterministic thermodynamics based on ensemble averages of bulk collections of molecules undergoing electrocatalysis.

Electron-transfer reactions

An STM by itself can provide two means of catalysing single-molecule reactions (Fig. 5a), one employing electrons[128,129] and the other electric fields[10,11,130,131]. Before we examine the mechanisms of electron-mediated reactions and electron catalysis, we first of all discuss how electrons exchange between electrodes and molecules. In solution-based chemistry, reductants such as Zn dust[132] and oxidants such as $FeCl_3$ (ref.[133]) are often used to inject electrons and holes, respectively, into reactants. At the single-molecule level, the electrode is the ideal electron or hole source to initiate chemical reactions. Depending on the energy of the electrons, electron-mediated single-molecule reactions can be classified into two categories.

For the low-energy case (Fig. 5b) in the inelastic tunnelling regime, electrons are injected into the molecule in such a way so as to excite[134,135] its vibrational modes, leading to energy exchange between the electrons and the bonds in the molecule. Bond breaking occurs when the transferred energy exceeds the bond dissociation barrier. Some pioneering experiments — such as the intramolecular bond dissociations of O–O bonds[135], C–H bonds[134] and C–I[129] bonds, and hydrogen tautomerization in melamine[136] and napthocyanine[137] derivatives — have confirmed the involvement of a vibrational excitation mechanism. Inelastic electron tunnelling is realized by positioning the STM tip above the bond of interest and then dosing it with electrons at a fixed height so as to perform single-molecule chemistry with single-bond resolution.

For the high-energy case (Fig. 5c) in the field-emission regime, electrons are transferred to an unoccupied orbital in the molecule, raising it to a high-energy electronic state. Such electron-transfer processes and the corresponding charge-state changes in a molecule govern[122] its aromaticity and reactivity and have implications for electro- and photocatalysis. For example, when an electron is injected[138,139] into the antibonding level of O_2, the O=O bond breaks owing to the generation of activated negatively charged states. Such electron-transfer processes follow very closely the catalytic mechanisms employed in organic electrochemical synthesis[14,140] carried out in solution — where the formation of radical[141] or cationic[142] intermediates is the key step — suggesting yet another way to investigate electrocatalytic routes at the single-molecule level.

Single-molecule redox reactions

Adding (or removing) electrons to (or from) a single molecule can be promoted in three-terminal solid-state devices[143,144] or in electrochemical cells[145,146]. The gate voltage scan offers[147] an integrated approach to tuning the relative positions of the molecular orbitals with respect to the electrode Fermi level, promoting the injection (subtraction) of electrons into (from) the SMJs, and creating different charge states in a single molecule, finally leading to detectable changes in single-molecule conductance. In particular, a single-molecule electrochemical platform provides[148] complementary approaches to understanding electron transfer in redox-active molecules, mimicking the electrochemical reactions that take place in bulk solutions. Several milestones in this area have been achieved by using redox-active molecules, such as naphthalene or perylenediimide[149–151], anthraquinone[152,153], viologens[154–156], tetrathiafulvalene[157,158], benzodifuran[159], the thieno derivative of bifluorenylidene[160], transition metal complexes[161,162] and even single-cluster junctions[163].

In a typical four-electrode single-molecule electrochemical cell based on the STM break-junction platform (Fig. 5d), the STM break-junction tip and substrate serve as the two working electrodes. The incorporation of counter and reference electrodes controls the electrochemical potential of the tip and substrate. The potential difference between these two working electrodes is also the bias voltage applied across the molecular junction, driving the tunnelling current to flow through the single molecule. Such an implementation can be compared with the conventional three-electrode cell (Fig. 5e) used in ensemble electrochemical experiments. It remains unclear how the insights gained from mechanisms identified in individual electron-transfer reactions relate to ensemble measurements. According to different mechanisms of electron transfer at the molecular level, single-molecule redox reactions can be categorized into three sets.

First, in macroscopic electrochemistry, the Butler–Volmer equation[164] is one of the most fundamental pieces of theory that is used (Fig. 5f) to describe relationships between the electrode potentials

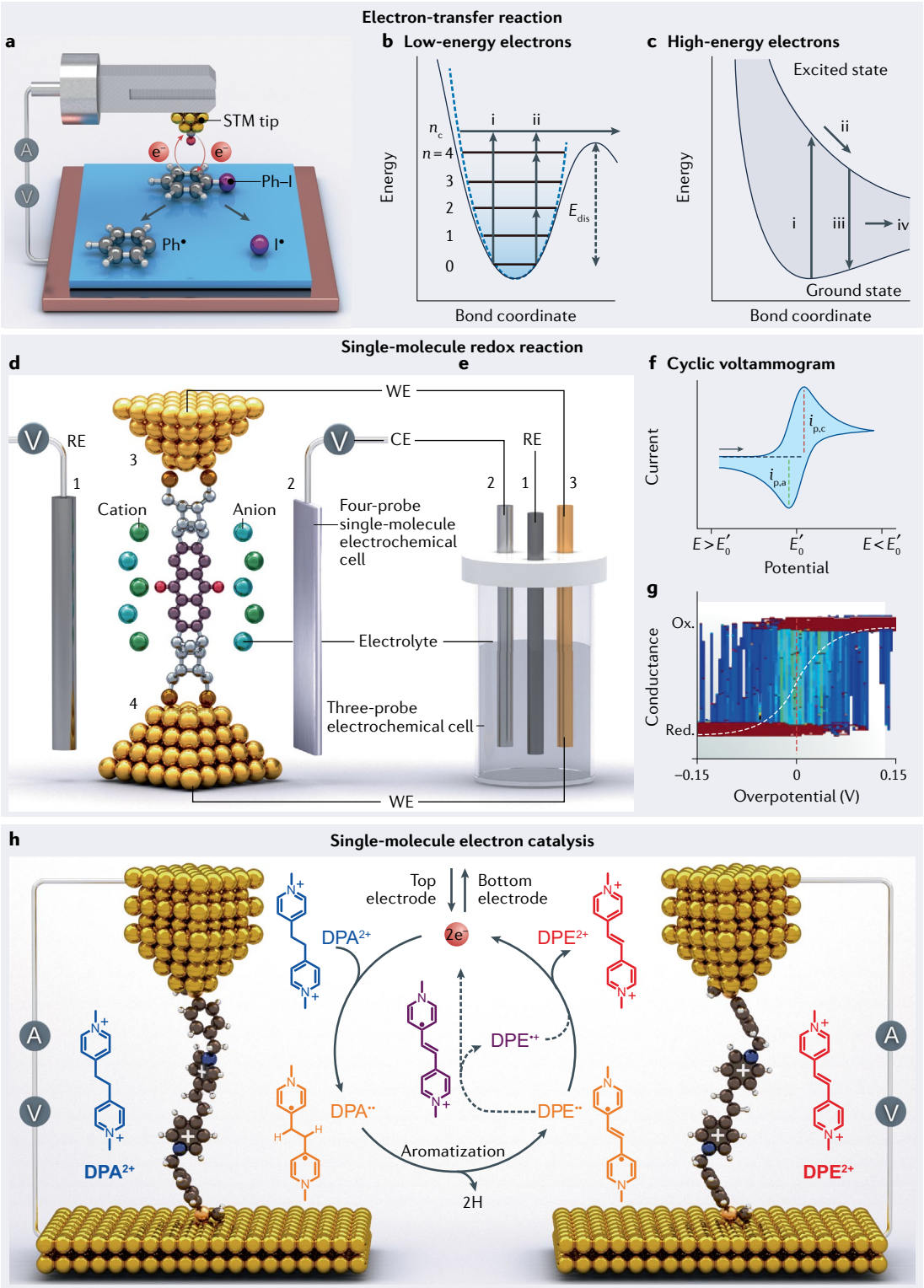

and current densities that govern redox-reaction kinetics. At the single-molecule level, however, each electron-transfer process is stochastic and exhibits[165] (Fig. 5g) large conductance fluctuations between the reduced and oxidized states. The probability of single-molecule fluctuations follows the first-order kinetics described by the Butler–Volmer equation. Ensemble averaging of conductance in relation to electrochemical potentials follows a sigmoidal dependence, which can be described by equilibrium electron transfer and the Nernst equation.

Fig. 5 | Single-molecule electron catalysis. a, The electron-induced abstraction of iodine from iodobenzene. **b**, Potential energy diagram of the model for bond breaking by low-energy inelastic electron tunnelling. (i) At high bias, the energy of one electron is sufficient for bond dissociation; (ii) at low bias, three electrons are required. **c**, Potential energy diagram of the four steps that lead to molecular fragmentation induced by high-energy electrons: (i) electron capture, (ii) nuclear relaxation, (iii) an electron returning to the ground state and the formation of a vibrationally excited state, which (iv) leads to the dissociation of covalent bonds. **d**, A four-probe single-molecule electrochemical cell based on STM break junctions. The tip and substrate of a STM break-junction setup serves as the two working electrodes. The use of counter and reference electrodes controls the electrochemical potential between the tip and the substrate. **e**, A typical electrochemical cell for ensemble-redox experiments in solution contacting three electrodes: a working electrode (WE), a counter electrode (CE) and a reference electrode (RE). These three electrodes are connected to a potentiostat, which applies a potential difference between the WE (where the electrochemical reaction takes place) and the RE (which serves as a stable reference point against the potentials of other electrodes). The CE completes the circuit and allows current to flow. **f**, A cyclic voltammogram for a solution undergoing a reversible one-electron redox reaction. **g**, Conductance–potential histograms showing large conductance fluctuations for a single-molecule electron-transfer reaction. **h**, Schematic illustration and a proposed reaction mechanism for an electron-catalysed single-molecule dehydrogenation. Two electrons are injected from the top electrode to DPA^{2+} and trigger the formation of a diradical, $DPA^{\bullet\bullet}$. This unstable diradical then transforms to another diradical, $DPE^{\bullet\bullet}$, through a dehydrogenation step. Two electrons are finally removed from $DPE^{\bullet\bullet}$ and moved to the bottom electrode, leading to the oxidative state of DPE^{2+} and the completion of the catalytic loop. DPA, 1,2-di(4-pyridinium) ethane backbone; DPE, 1,2-di(4-pyridinium)ethene backbone; E, electrochemical potential; E_0', reduction potential of the analyte; E_{dis}, dissociation barrier; $i_{p,c}$, cathodic current reaches a maximum at a potential ($E_{p,c}$) during the reduction of the analyte; $i_{p,a}$, anodic current reaches a maximum at a potential ($E_{p,a}$) during oxidation; n, vibrational quantum number; n_c, vibrational excitation level at which the bond breaks promptly; STM, scanning tunnelling microscope. Panel **b** adapted with permission from ref.[135], APS. Panel **c** adapted with permission from ref.[139], AAAS. Panel **g** adapted with permission from ref.[165], National Academy of Sciences. Panel **h** adapted with permission from ref.[175], copyright 2021 American Chemical Society.

Second, when the central redox centre is decoupled electronically from the electrode, the electron-transfer reaction prefers to follow a two-step hopping model[166] via the redox centre – that is, the electron transfers from the top electrode to the redox centre by a Franck–Condon transition, the molecule reorganizes as a result of environmental and internal relaxation in the adiabatic limit, and finally the electron transfers from the redox centre to the bottom electrode. When moving from positive overpotentials towards the negative direction, the conductance increases in the direction of the reversible potential and then decreases, giving a maximum molecular conductance close to the equilibrium redox potential.

Third, electrochemical reaction-induced structural changes result in new quantum phenomena – such as quantum interference – at the molecular level, leading to a large variation in conductance[152,153,167]. For example, the electrochemical potential sweep causes a redox-induced structural change between an oxidized anthraquinone and reduced hydroanthraquinone. The anthraquinone has a cross-conjugated backbone, leading to destructive quantum interference and lower conductance, whereas the quantum interference effect is absent in the linearly conjugated dihydroxyanthracene backbone. In this respect, the single-molecule electrochemical platform provides a unique way to inspect the structural transformations during electrochemical reactions and electron catalyses.

Single-molecule electron catalysis

The single-electron sensitivity of the ultrahigh-vacuum STM and non-contact AFM platforms reveals[168] insights into reaction pathways during electrocatalysis. In an ultrahigh-vacuum STM or non-contact AFM platform, however, these single-molecule reactions are typically performed[122,169,170] on defect-free metal substrates under ultrahigh-vacuum conditions and at cryogenic temperatures, situations which do not reflect the experimental conditions employed in homogeneous photo- or electrocatalysis. To achieve better comparisons between reactions performed at the single-molecule level and in bulk solution, the harsh operating conditions associated with STMs must be rendered milder to match the experimental conditions employed in photo- or electrocatalysis. For example, to investigate CO_2 conversion, the metal substrates typically used in STM can be replaced with TiO_2, a widely used photocatalyst[171]. STM results reveal that, for CO_2 to be adsorbed on TiO_2 substrates, electron-injection-induced generation of $CO_2^{\bullet-}$ is the decisive step in the CO_2 reduction to CO. This catalytic mechanism can guide the design of photocatalysts for CO_2 reduction[172] and H_2O splitting[173].

Moreover, when a single-molecule reactant is a good electron host[23,174], such as in the case of a dehydrogenation of 1,2-di(4-pyridinium)ethane[175], the electrons injected from the STM tip become trapped in the single molecule, triggering (Fig. 5h) the dehydrogenation before the electrons are extracted into the bottom substrate. Concepts can be borrowed from the chemistry of bulk reaction mechanisms[176] in order to elucidate the reactions of single molecules[139]. Electron catalysis can be recognized as a general class of chemical reactions that proceed slowly and routinely in solution under normal thermal conditions, and that can be accelerated by generating various reactive intermediates upon injection of electrons at appropriate electrochemical potentials. In the electron-catalysed single-molecule dehydrogenation, a linear relationship between redox energies (ΔE_r and ΔE_o) and tip/substrate bias voltages (V_t and V_s) can be obtained qualitatively. An increase in bias voltage elevates the energy level of electrons in the tip, while pushing down the energy level of the electrons in the substrate. Compared with ensemble reactions in solution, the STM break-junction platform provides an ultrahigh electric field that is directed along the molecular backbone, causing the energy to decrease from −7.11 to −8.86 kcal mol^{-1} and thus promoting the dehydrogenation in a thermodynamic manner.

Electric field catalysis

The ability of electric fields to affect the reactivities and selectivities of non-redox reactions – long anticipated by both theoretical and experimental chemists – has emerged[10,177] as a viable form of chemical catalysis during the past 5 to 10 years. Electric field catalysis is at the heart of some biological enzymatic reactions[178], occurring naturally when reactants constitute[179,180] (Fig. 6a) an optimal match at sites relative to charged units inside. For electric field catalysis to be exploited in the domain of synthetic chemistry, the obvious challenge is how to align the molecules and electric fields. One solution is to mimic[181] the active sites of enzymes by synthesizing[182] a supramolecular container that generates an electric field inside its cavity, and then encapsulating[183,184] reactants inside the nanoconfined space to align with the field and alter their reactivity[185,186] (Fig. 6b).

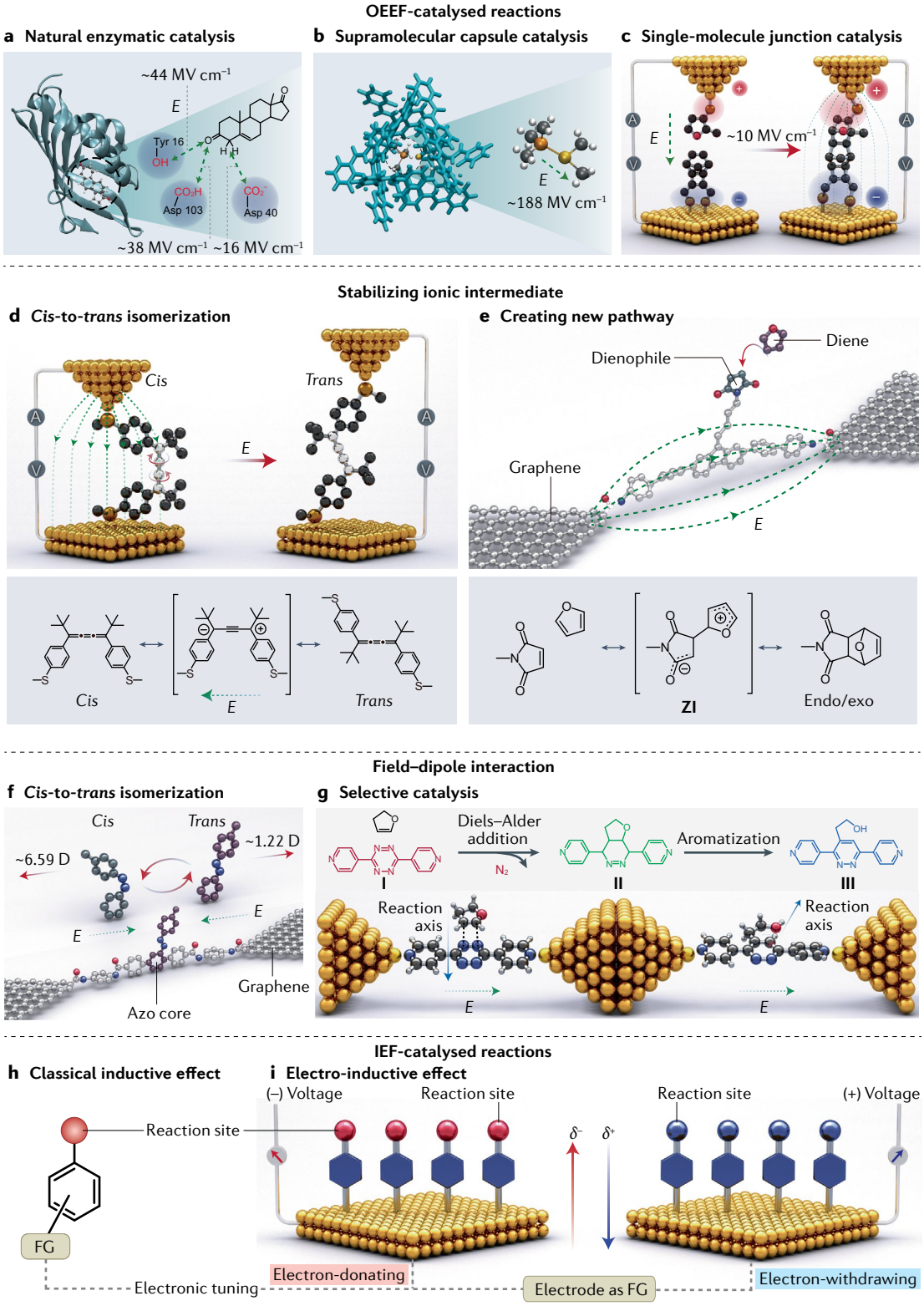

Another solution is to use[20] a break-junction platform through which a directional electric field can be applied (Fig. 6c), allowing the links between electric fields and the kinetics and/or dynamics of chemical reactions at SMJs to be investigated quantitatively. Depending on the conditions under which break-junction experiments are performed and how electric fields are generated, these reactions can

Fig. 6 | Single-molecule electric field catalysis. a, Natural enzymatic catalysis by the electric field *E* generated in the active site of a ketosteroid isomerase by three amino acid residues. **b**, Supramolecular capsule catalysis by the electric field generated inside a nanocage and projected onto the gold–alkyl ligand bonds of an encapsulated guest. **c**, A Diels–Alder reaction catalysed by an electric field generated between the two electrodes in a scanning tunnelling microscope (STM). **d**, Electric-field-catalysed *cis*-to-*trans* isomerization of [3]cumulene. The reaction proceeds because electric fields stabilize the zwitterionic resonance structure of *cis*[3]cumulene. **e**, Electric field-created stepwise reaction pathway for a Diels–Alder reaction. The stepwise Diels–Alder reaction proceeds because electric fields stabilize the zwitterionic intermediate state **ZI**. **f**, Schematic illustration showing an azobenzene single-molecule junction bridging two graphene electrodes. The azobenzene undergoes reversible *cis*-to-*trans* isomerization induced by field–dipole interactions. **g**, The electric-field-induced selective catalysis of a two-step cascade reaction. Step 1: a Diels–Alder cycloaddition (**I**→**II**) between 2,3-dihydrofuran (**I**) and a tetrazine derivative (**II**) with concomitant loss of N_2. Step 2: an aromatization (**II**→**III**) to give a pyridazine derivative (**III**). The reaction axis of the Diels–Alder reaction is orthogonal to the electric field, while the reaction axis for aromatization is nonorthogonal to the electric field. **h**, The classical inductive effect uses a functional group (FG) to electronically tune a molecule in order to manipulate the reactivity of a reaction site. **i**, In the electro-inductive effect, an electrode acts as the FG to electronically tune an active reaction site of a single molecule, realized by applying different potentials to the electrode. IEF, interfacial electric field; OEEF, oriented external electric field. Panel **a** adapted with permission from ref.[180], copyright 2019 American Chemical Society. Panel **b** adapted from ref.[181], Springer Nature Limited. Panel **c** adapted from ref.[20], Springer Nature Limited. Panel **d** adapted from ref.[190], CC BY 4.0 (https://creativecommons.org/licenses/by/4.0/). Panel **f** adapted from ref.[21], CC BY 4.0 (https://creativecommons.org/licenses/by/4.0/).

be classified into two categories: reactions[10,130,131] catalysed by oriented external electric fields (OEEFs), generated within the nanogap between the STM electrodes; and reactions[187–189] initiated by interfacial electric fields (IEFs), originating from electrical double layers in electrochemical cells.

OEEF-catalysed reactions

By applying a large external electric field over a small distance between two STM electrodes, a 2016 experiment[20] demonstrated that it was possible to direct and catalyse single-molecule Diels–Alder reactions (Fig. 6c). Since then, electric fields generated between STM electrodes have provided glimpses of wide-ranging possibilities for manipulating[10,130] the potential energy of different species along reaction coordinates, affecting the kinetics, thermodynamics and selectivities of chemical reactions, as well as exploring solvent effects on chemical reactions (Box 3).

First, OEEFs have a catalytic effect because they induce and stabilize the ionicity of bonds in intermediates and transition states, thereby decreasing the kinetic barriers to reactions under investigation. For example, the isomerizations of [3]cumulene derivatives have relatively high energy barriers that cannot be overcome by simply heating or irradiating the derivatives in solution. The existence of an electric field[190], however, stabilizes the polar zwitterionic resonance structures of the derivatives (Fig. 6d), reducing the rotational barriers and making the *cis*-to-*trans* isomerizations energetically accessible enough to proceed in solution. Regulating the electric field strength is also a powerful tool for manipulating reaction rates and alternating between different reaction pathways. Consider the Diels–Alder reaction portrayed in ref.[55] (Fig. 6e). Under the influence of an electric field, it adopts a different pathway from the conventional concerted mechanism — namely, it undergoes a stepwise cycloaddition in which one bond is formed between a diene and a dienophile to give a charge-separated zwitterionic intermediate **ZI**. The lifetime of **ZI** and the probability of stepwise pathways can be regulated by the electric field strength, thus allowing the manipulation of reaction mechanisms.

Second, changing the orientation of an OEEF can lead to the unique tuning of the catalytic selectivity of a reaction. Aligning the direction of the electric field along the reaction axis of an activated bond — that is, the dipole moment of the molecule — induces a particular chemical reaction. The field–dipole interaction (Fig. 6f) has been verified[21] experimentally in the electric-field-catalysed isomerization of azobenzene derivatives. Different directions of electric fields produce an asymmetric selectivity for the two azobenzene configurational isomers: the positive bias prefers the *trans* form, whereas a large negative bias favours the *cis* form. When an electric field is applied to a two-step cascade reaction[61] — a Diels–Alder cycloaddition (Fig. 6g, **I**→**II**) followed by an aromatization (Fig. 6g, **II**→**III**) — the Diels–Alder reaction remains unaffected because its reaction axis is orthogonal to the electric field, whereas the rate of aromatization is accelerated by one order of magnitude because its reaction axis is aligned along the field. This orientation-selective catalytic effect of OEEFs demonstrates that chemical reactions can be controlled selectively and in a stepwise manner by precise alignment between external electric fields and reaction trajectories.

IEF-catalysed reactions

The SMJ technique has the potential to be applied as a toolkit for organic synthesis based on the experimental fact that the electric fields applied across the nanogap of an STM can affect not only the fraction of reactants forming molecular junctions, but also those free molecules close to the junctions in solution[190,191]. The solution around the tip and substrate area is exposed to ultrahigh electric fields on account of the diffusion of molecules and solvents, as well as local turbulence induced by movements of the STM tip. To find a general and reliable way to expand the scale of electric field catalysis from SMJs to bulk solutions, electrochemical cells — usually used in Faradaic reactions — can be employed to generate ultrahigh IEFs to manipulate the reactivities and selectivities of non-Faradaic reactions. We focus on recent progress in IEF-catalysed reactions. More comprehensive discussions can be found in other reviews[131,192].

When a positive bias is applied to a gold electrode, the anions are drawn close to the surface and all cations are repelled away from it. Consequently, the local concentration of anions increases, whereas the concentration of cations decreases, establishing an electrochemical double layer at the electrode/electrolyte interface. The Gouy–Chapman model can estimate[193] the width (λ_D) of the double layer. Experimentally, the electric field distribution at the electrode–electrolyte interface can be probed using electrochemistry[194,195] or Raman spectroscopy[196,197]. Then, the IEF can be estimated as $E = V_{bias}/\lambda_D$. Like OEEF catalysis, IEF catalysis arises from the stabilization[188,189] of ionic structures associated with reaction intermediates, and it has been applied successfully to bond cleavages[187], bond formations[198], epoxide rearrangements[188] and carbene reactions[189].

When electrochemical STM break-junction measurements are performed in electrolytes, the STM tip must be coated with an insulating wax layer to lower the background ionic currents. The disparate areas of the two electrodes — the tip and the substrate — create an asymmetrical

Box 3

Solvent effects in single-molecule reactions

One of the big advantages of single-molecule junction (SMJ) platforms over other techniques, such as gas-phase or vacuum studies, is that solvents are involved in junction chemistry. From the perspective of experiments, there are three models we need to explore in order to understand solvent effects in single-molecule reactions. Solvent polarities provide local electric fields (see the figure, panels **a**–**c**) that can affect the reaction kinetics of single-molecule reactions.

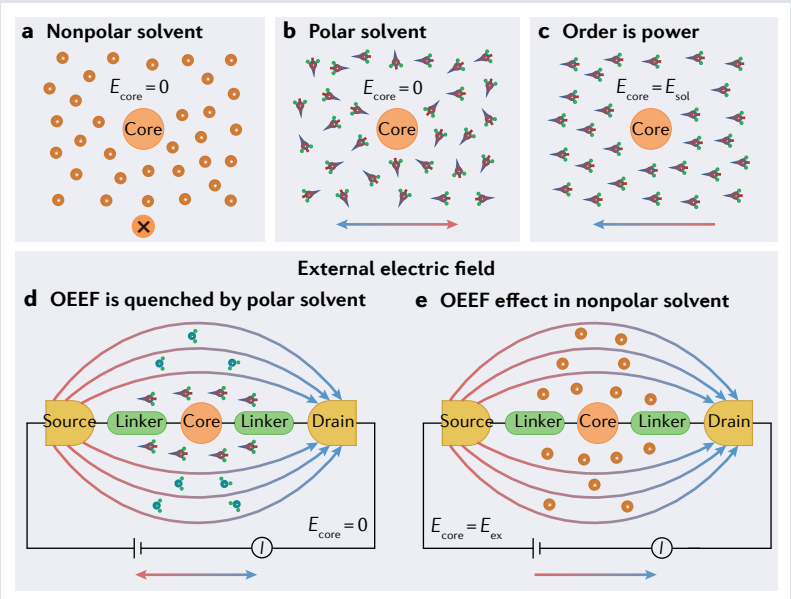

Polar solvents

In the case of conventional polar solvents (see the figure, panel **b**), a net electric field of zero is generated at equilibrium on account of the random movement of the solvent molecules. Despite the zero global electric field, the local electric field[231] induced by the polar solvent itself takes on the role of stabilizing polar species during chemical reactions. For example, in the case of single-molecule nucleophilic addition[51], water accelerates the reaction by stabilizing the polar amine oxide transition state.

Ordered polar solvents

In an ideal theoretical model, if solvent molecules are oriented[232] in an orderly fashion without the implementation of an external field, the accumulation of molecular dipoles will produce extremely large electric field strengths and thus provide the effect of electrostatic catalysis. All these theoretically proposed ideas, once implemented, could suggest new reaction conditions in future ensemble chemistry.

External electric fields and polar solvents

Oriented external electric fields (OEEFs) applied between electrodes can be screened[131] by polar solvents. Polar solvent molecules — with their dipole moments — can be oriented (see the figure, panel **d**) along the direction of the OEEF generated between source and drain electrodes in which the molecular junction is immersed. The alignment of polar solvent molecules generates[231] a reverse built-in electric field and quenches[23] the OEEF, at least partially if not completely, at SMJs. In the case of nonpolar solvents (see the figure, panel **e**), there are no field–dipole interactions between the OEEF and solvent molecules, enabling[131] the investigation of OEEF-catalysed reaction mechanisms.

distribution of cations around the tip. This distribution polarizes[199] the tip electrode owing to the formation of a dense double layer of charges in small areas exposed to solvents. On applying[31] a negative bias to the tip electrode, the chemical potential increases, making it electron-rich. Then, the tip electrode can promote electron donation from Au to the molecule, leading to bond formation[31,62].

The polarization of asymmetric electrodes can also be viewed as an electro-inductive effect in the STM. In this situation, the Hammett relationship[200] — used by organic chemists to quantify the electron-donating or -withdrawing properties of functional groups in homogeneous chemistry — can be borrowed to interpret[201–203] the electronic polarization induced by biased electrodes in heterogeneous chemistry. In homogeneous chemistry, the electronic characteristics of molecules can be regulated (Fig. 6h) by the presence of different functional groups. For example, in a single-molecule Suzuki–Miyaura cross-coupling[56], the inductive effect of substituents on reaction rates can be determined by inserting different functional groups at the *para*-position of the aromatic boronic acid. According to the Hammett relationship[203], the linear fit between $\log(k_X/k_H)$ and the *para*-substituent constant σ_p leads to a Hammett constant of +3.34, demonstrating that electron-withdrawing substituents on the boronic acid accelerate the Suzuki–Miyaura cross-coupling.

We can extend (Fig. 6i) the classical inductive effect to heterogeneous chemistry by replacing the chemical tuning groups with biased electrodes[202]. The electronic properties of molecules can be modulated by changing the applied voltages at the attached electrodes. Negative potentials are applied to imitate electron-donating groups, whereas positive potentials simulate electron-withdrawing groups. Unlike the classical inductive effect, the electro-inductive effect is not discrete because bias voltages can be varied continuously. There is no need to synthesize a series of analogous reactants or catalysts to impose different inductive effects on reactions, an advantage for producing chemical products in a more efficient manner. Employing the paradigm that electrodes can act as functional groups, a Suzuki–Miyaura cross-coupling has been performed[202] on the surface of gold electrodes.

Future perspectives

Looking to the future, and given the creativity of researchers worldwide, we can almost certainly expect to witness inroads being made into other areas of single-molecule reactions, such as capturing excitation and transition states, making connections between conductance and other single-molecule properties, and leveraging single-molecule reactions to produce materials in a practical and scalable way. What are the challenges?

Experimental caution and future challenges

Many factors influencing single-molecule reactions must be considered because of the complexity of reactions at the single-molecule level. A variety of control experiments are necessary in order to determine the mechanisms that dominate the catalysis, such as those induced by metal electrodes, mechanical force, thermal heat, electron tunnelling excitation or resonant transport in molecular junctions. For example, when metals are used as electrodes in STM measurements — in addition to enabling catalysis by tunnelling electrons or local electric field — a fact that cannot be ignored is that the metal electrode itself can act as a catalyst[204]. Monomers have been reported to dimerize[29] and trimerize[204] covalently in SMJs, demonstrating the catalytic capability of gold atoms or nanoparticles that have been peeled off STM electrodes. The catalytic performance of metal electrodes also depends on their compositions and morphologies, but it is not easy to control these features — and hence the catalytic ability — of STM tips. More delicate experiments are needed to explore the specific impact of these factors on catalytic effects to establish a model system that is closer to the actual catalytic environment. A more challenging situation is the investigation of the competing or synergistic effects of two or more catalytic conditions when developing new synthetic methodologies.

Increasing temporal resolution

Developing ultrafast real-time measurement platforms, especially those that can be used in solution under ambient conditions, remains a long-standing goal to help characterize intermediates and transition states. Break-junction techniques, although now a powerful reaction platform, fail to provide good temporal resolution. The sampling rate is on a timescale of microseconds, which is far from capturing reaction intermediates or transition states. More attention needs to be paid to improving[205] the acquisition rates to nanoseconds and decreasing the electrical and vibrational noise in order to capture transient phenomena. Another approach could be to integrate the electrical SMJ platforms with ultrafast laser spectroscopy to investigate the molecular structure dynamics and electron-transfer processes of photochemical reactions on the extremely short timescale of picoseconds. Furthermore, we anticipate a strong union between single-molecule testbeds and machine-learning algorithms when handling large amounts of complex real-time data in order to increase the accuracy, scalability and controllability of the measurements.

Integrating with other methods

Combining single-molecule testbeds based on electrical currents with other methods would capture the advantages of both techniques and advance our understanding of structure–function relationships in single-molecule reactions. For example, employing single-molecule electroluminescence[206] or super-molecule-resolution fluorescence[56,207] could help to locate the positions of specific molecules in a device. The location of a single molecule can be realized by combining a stochastic optical reconstruction microscope with high-speed sampling of current detection platforms. Successive reactions taking place at the kernel of a molecular junction induce fluorescence blinking at the catalytic site, on account of the nonradiative energy and charge transfer from the catalytic centre to the electrodes. Other spectroscopic platforms such as Raman[208], infrared[209], and terahertz[210] spectroscopy can provide fingerprint-like information about bond cleavage or formation during single-molecule reactions, leading to more information, precision and new readout variables. In contrast with the electrical signal provided by the SMJ technique, these spectroscopic methods offer orthogonal platforms based on different modes of energy transitions. Experimentally, these spectroscopic signals can be measured simultaneously along with electrical signals, providing real-time spectral information related to electrical signals during single-molecule reactions.

Going beyond characterizing electronic transport and introducing other techniques, such as single-molecule manipulation, may increase signal resolution. We propose three directions worth exploring. First, we recommend using optical-trapping techniques[211,212] to control the location of single molecules in electrode nanogaps. Manipulation of a single-molecule reactant is challenging but is, nonetheless, worth investigating, with the prospect of encountering the randomizing effect of Brownian motion during reactions in solution. Second, we recommend employing superfast and ultracold techniques[213] to enable the manipulation and measurement of excited states. Achievements in this direction will provide fundamental knowledge about electron and energy transfer processes during single-molecule transformations. Third, we recommend combining single-molecule imaging platforms[214] with current measurement techniques in order to provide atomic-scale spatial resolution and spectroscopic information associated with chemical bond transformations.

Connecting single-molecule insights to bulk reactions

The gap between single-molecule and bulk reactions also needs to be bridged. Translating[7,9] single-molecule investigations into improved bulk-scale synthesis is difficult. The goal of SMJ reactions is ultimately to harness and scale up the effects of electron and electric field catalysis to deliver products on the kilogram scale. For example, by transforming electric field catalysis in SMJs into interfacial electric catalysis in electrochemical cells, we can expect to transform the research paradigm from the single-molecule to the monolayer level. In addition, the electro-inductive effect of electrodes in interfacial electric field catalysis can be utilized to modulate the electronic structures of reactants or catalysts over the course of a catalytic cycle, enabling fine control over the progress of chemical reactions by applying sequential voltages. Another direction worth exploring is to integrate electron or electric field catalysis with flow microreactor technology, with the aim of scaling up single-molecule reactions[215,216]. STM tips can be replaced by arrays of metal electrodes prepared by nanofabrication methods. The micrometre-scale channels in flow-cell chips can provide rapid and controllable mass transport, enabling continuous reactions in the vicinity of electrodes. Large-scale production of materials can be realized by absorbing the unreacted reactants and desorbing the products, rendering reactions recyclable.

Published online: 2 December 2022

References

1. Chen, P. et al. Single-molecule fluorescence imaging of nanocatalytic processes. *Chem. Soc. Rev.* **39**, 4560–4570 (2010).
2. Vogt, E. T. C. & Weckhuysen, B. M. Fluid catalytic cracking: recent developments on the grand old lady of zeolite catalysis. *Chem. Soc. Rev.* **44**, 7342–7370 (2015).

3. Wang, B. et al. From the molecule to the mole: improving heterogeneous copper catalyzed click chemistry using single molecule spectroscopy. *Chem. Commun.* **53**, 328–331 (2017).
4. Chen, T. et al. Optical super-resolution imaging of surface reactions. *Chem. Rev.* **117**, 7510–7537 (2017).
5. Wang, W. Imaging the chemical activity of single nanoparticles with optical microscopy. *Chem. Soc. Rev.* **47**, 2485–2508 (2018).
6. Dong, B., Mansour, N., Huang, T.-X., Huang, W. & Fang, N. Single molecule fluorescence imaging of nanoconfinement in porous materials. *Chem. Soc. Rev.* **50**, 6483–6506 (2021).
7. Eivgi, O. & Blum, S. A. Exploring chemistry with single-molecule and -particle fluorescence microscopy. *Trends Chem.* **4**, 5–14 (2022).
8. Cordes, T. & Blum, S. A. Opportunities and challenges in single-molecule and single-particle fluorescence microscopy for mechanistic studies of chemical reactions. *Nat. Chem.* **5**, 993–999 (2013).
9. Scaiano, J. C. & Lanterna, A. E. Is single-molecule fluorescence spectroscopy ready to join the organic chemistry toolkit? A test case involving click chemistry. *J. Org. Chem.* **82**, 5011–5019 (2017).
10. Shaik, S., Mandal, D. & Ramanan, R. Oriented electric fields as future smart reagents in chemistry. *Nat. Chem.* **8**, 1091–1098 (2016).
11. Shaik, S., Danovich, D., Joy, J., Wang, Z. & Stuyver, T. Electric-field mediated chemistry: uncovering and exploiting the potential of (oriented) electric fields to exert chemical catalysis and reaction control. *J. Am. Chem. Soc.* **142**, 12551–12562 (2020).
12. Huang, X. & Li, T. Recent progress in the development of molecular-scale electronics based on photoswitchable molecules. *J. Mater. Chem. C* **8**, 821–848 (2020).
13. Twilton, J. et al. The merger of transition metal and photocatalysis. *Nat. Rev. Chem.* **1**, 0052 (2017).
14. Yan, M., Kawamata, Y. & Baran, P. S. Synthetic organic electrochemical methods since 2000: on the verge of a renaissance. *Chem. Rev.* **117**, 13230–13319 (2017).
15. Rutledge, H. L. & Tezcan, F. A. Electron transfer in nitrogenase. *Chem. Rev.* **120**, 5158–5193 (2020).
16. Joachim, C., Gimzewski, J. K. & Aviram, A. Electronics using hybrid-molecular and mono-molecular devices. *Nature* **408**, 541–548 (2000).
17. Flood, A. H., Stoddart, J. F., Steuerman, D. W. & Heath, J. R. Whence molecular electronics? *Science* **306**, 2055–2056 (2004).
18. Joachim, C. & Ratner, M. A. Molecular electronics: some views on transport junctions and beyond. *Proc. Natl Acad. Sci. USA* **102**, 8801–8808 (2005).
19. Xiang, D., Wang, X., Jia, C., Lee, T. & Guo, X. Molecular-scale electronics: from concept to function. *Chem. Rev.* **116**, 4318–4440 (2016).
20. Aragonès, A. C. et al. Electrostatic catalysis of a Diels–Alder reaction. *Nature* **531**, 88–91 (2016).
21. Meng, L. et al. Side-group chemical gating via reversible optical and electric control in a single molecule transistor. *Nat. Commun.* **10**, 1450 (2019).
22. Gehring, P., Thijssen, J. M. & van der Zant, H. S. J. Single-molecule quantum-transport phenomena in break junctions. *Nat. Rev. Phys.* **1**, 381–396 (2019).
23. Chen, H. et al. Single-molecule charge transport through positively charged electrostatic anchors. *J. Am. Chem. Soc.* **143**, 2886–2895 (2021).
24. Li, X. et al. Supramolecular systems and chemical reactions in single-molecule break junctions. *Top. Curr. Chem.* **375**, 42 (2017).
25. Stone, I. et al. A single-molecule blueprint for synthesis. *Nat. Rev. Chem.* **5**, 695–710 (2021).
26. Xie, X. et al. Single-molecule junction: a reliable platform for monitoring molecular physical and chemical processes. *ACS Nano* **16**, 3476–3505 (2022).
27. Li, Y., Yang, C. & Guo, X. Single-molecule electrical detection: a promising route toward the fundamental limits of chemistry and life science. *Acc. Chem. Res.* **53**, 159–169 (2020).
28. Cheng, Z. L. et al. In situ formation of highly conducting covalent Au–C contacts for single-molecule junctions. *Nat. Nanotechnol.* **6**, 353–357 (2011).
29. Chen, W. et al. Highly conducting π-conjugated molecular junctions covalently bonded to gold electrodes. *J. Am. Chem. Soc.* **133**, 17160–17163 (2011).
30. Hines, T. et al. Controlling formation of single-molecule junctions by electrochemical reduction of diazonium terminal groups. *J. Am. Chem. Soc.* **135**, 3319–3322 (2013).
31. Starr, R. L. et al. Gold–carbon contacts from oxidative addition of aryl iodides. *J. Am. Chem. Soc.* **142**, 7128–7133 (2020).
32. Doud, E. A. et al. In situ formation of N-heterocyclic carbene-bound single-molecule junctions. *J. Am. Chem. Soc.* **140**, 8944–8949 (2018).
33. Zang, Y. et al. Electronically transparent Au–N bonds for molecular junctions. *J. Am. Chem. Soc.* **139**, 14845–14848 (2017).
34. Lamberti, C., Zecchina, A., Groppo, E. & Bordiga, S. Probing the surfaces of heterogeneous catalysts by in situ IR spectroscopy. *Chem. Soc. Rev.* **39**, 4951–5001 (2010).
35. Blasco, T. Insights into reaction mechanisms in heterogeneous catalysis revealed by in situ NMR spectroscopy. *Chem. Soc. Rev.* **39**, 4685–4702 (2010).
36. Wasielewski, M. R. Photoinduced electron transfer in supramolecular systems for artificial photosynthesis. *Chem. Rev.* **92**, 435–461 (1992).
37. Xu, W., Kong, J. S., Yeh, Y.-T. E. & Chen, P. Single-molecule nanocatalysis reveals heterogeneous reaction pathways and catalytic dynamics. *Nat. Mater.* **7**, 992–996 (2008).
38. Xiao, Y. et al. Revealing kinetics of two-electron oxygen reduction reaction at single-molecule level. *J. Am. Chem. Soc.* **142**, 13201–13209 (2020).
39. Zhou, X., Xu, W., Liu, G., Panda, D. & Chen, P. Size-dependent catalytic activity and dynamics of gold nanoparticles at the single-molecule Level. *J. Am. Chem. Soc.* **132**, 138–146 (2010).
40. Liu, X. et al. Revealing the catalytic kinetics and dynamics of individual Pt atoms at the single-molecule level. *Proc. Natl Acad. Sci. USA* **119**, e2114639119 (2022).
41. Rybina, A. et al. Distinguishing alternative reaction pathways by single-molecule fluorescence spectroscopy. *Angew. Chem. Int. Ed.* **52**, 6322–6325 (2013).
42. Kim, D., Zhang, Z. & Xu, K. Spectrally resolved super-resolution microscopy unveils multipath reaction pathways of single spiropyran molecules. *J. Am. Chem. Soc.* **139**, 9447–9450 (2017).
43. Ramsay, W. J., Bell, N. A. W., Qing, Y. & Bayley, H. Single-molecule observation of the intermediates in a catalytic cycle. *J. Am. Chem. Soc.* **140**, 17538–17546 (2018).
44. Zaera, F. Probing liquid/solid interfaces at the molecular level. *Chem. Rev.* **112**, 2920–2986 (2012).
45. Roeffaers, M. B. J. et al. Spatially resolved observation of crystal-face-dependent catalysis by single turnover counting. *Nature* **439**, 572–575 (2006).
46. van Schrojenstein Lantman, E. M., Deckert-Gaudig, T., Mank, A. J. G., Deckert, V. & Weckhuysen, B. M. Catalytic processes monitored at the nanoscale with tip-enhanced Raman spectroscopy. *Nat. Nanotechnol.* **7**, 583–586 (2012).
47. Choi, H.-K. et al. Single-molecule surface-enhanced Raman scattering as a probe of single-molecule surface reactions: promises and current challenges. *Acc. Chem. Res.* **52**, 3008–3017 (2019).
48. Zhan, C. et al. From plasmon-enhanced molecular spectroscopy to plasmon-mediated chemical reactions. *Nat. Rev. Chem.* **2**, 216–230 (2018).
49. Zhan, C., Chen, X.-J., Huang, Y.-F., Wu, D.-Y. & Tian, Z.-Q. Plasmon-mediated chemical reactions on nanostructures unveiled by surface-enhanced Raman spectroscopy. *Acc. Chem. Res.* **52**, 2784–2792 (2019).
50. Zhan, C., Moskovits, M. & Tian, Z.-Q. Recent progress and prospects in plasmon-mediated chemical reaction. *Matter* **3**, 42–56 (2020).
51. Guan, J. et al. Direct single-molecule dynamic detection of chemical reactions. *Sci. Adv.* **4**, eaar2177 (2018).
52. Nicolai, C. & Sachs, F. Solving ion channel kinetics with the QuB software. *Biophys. Rev. Lett.* **08**, 191–211 (2013).
53. Gu, C. et al. Label-free dynamic detection of single-molecule nucleophilic-substitution reactions. *Nano Lett.* **18**, 4156–4162 (2018).
54. Yang, C. et al. Single-molecule electrical spectroscopy of organocatalysis. *Matter* **4**, 2874–2885 (2021).
55. Yang, C. et al. Electric field–catalyzed single-molecule Diels–Alder reaction dynamics. *Sci. Adv.* **7**, eabf0689 (2021).
56. Yang, C. et al. Unveiling the full reaction path of the Suzuki–Miyaura cross-coupling in a single-molecule junction. *Nat. Nanotechnol.* **16**, 1214–1223 (2021).
57. Xu, B. & Tao, N. Measurement of single-molecule resistance by repeated formation of molecular junctions. *Science* **301**, 1221–1223 (2003).
58. Venkataraman, L., Klare, J. E., Nuckolls, C., Hybertsen, M. S. & Steigerwald, M. L. Dependence of single-molecule junction conductance on molecular conformation. *Nature* **442**, 904–907 (2006).
59. Huang, C. et al. Single-molecule detection of dihydroazulene photo-thermal reaction using break junction technique. *Nat. Commun.* **8**, 15436 (2017).
60. Xiang, L. et al. Gate-controlled conductance switching in DNA. *Nat. Commun.* **8**, 14471 (2017).
61. Huang, X. et al. Electric field-induced selective catalysis of single-molecule reaction. *Sci. Adv.* **5**, eaaw3072 (2019).
62. Zang, Y. et al. In situ coupling of single molecules driven by gold-catalyzed electrooxidation. *Angew. Chem. Int. Ed.* **58**, 16008–16012 (2019).
63. Tang, C. et al. Identifying the conformational isomers of single-molecule cyclohexane at room temperature. *Chem* **6**, 2770–2781 (2020).
64. Albrecht, T., Slabaugh, G., Alonso, E. & Al-Arif, S. M. M. R. Deep learning for single-molecule science. *Nanotechnology* **28**, 423001 (2017).
65. Lemmer, M., Inkpen, M. S., Kornysheva, K., Long, N. J. & Albrecht, T. Unsupervised vector-based classification of single-molecule charge transport data. *Nat. Commun.* **7**, 12922 (2016).
66. Hamill, J. M., Zhao, X. T., Mészáros, G., Bryce, M. R. & Arenz, M. Fast data sorting with modified principal component analysis to distinguish unique single molecular break junction trajectories. *Phys. Rev. Lett.* **120**, 016601 (2018).
67. Lauritzen, K. P., Magyarkuti, A., Balogh, Z., Halbritter, A. & Solomon, G. C. Classification of conductance traces with recurrent neural networks. *J. Chem. Phys.* **148**, 084111 (2018).
68. Cabosart, D. et al. A reference-free clustering method for the analysis of molecular break-junction measurements. *Appl. Phys. Lett.* **114**, 143102 (2019).
69. Huang, F. et al. Automatic classification of single-molecule charge transport data with an unsupervised machine-learning algorithm. *Phys. Chem. Chem. Phys.* **22**, 1674–1681 (2020).
70. Fu, T., Zang, Y., Zou, Q., Nuckolls, C. & Venkataraman, L. Using deep learning to identify molecular junction characteristics. *Nano Lett.* **20**, 3320–3325 (2020).
71. Huang, B., Li, Z. & Li, J. An artificial intelligence atomic force microscope enabled by machine learning. *Nanoscale* **10**, 21320–21326 (2018).
72. Rashidi, M. & Wolkow, R. A. Autonomous scanning probe microscopy in situ tip conditioning through machine learning. *ACS Nano* **12**, 5185–5189 (2018).
73. Krull, A., Hirsch, P., Rother, C., Schiffrin, A. & Krull, C. Artificial-intelligence-driven scanning probe microscopy. *Commun. Phys.* **3**, 54 (2020).

74. de Almeida, A. F., Moreira, R. & Rodrigues, T. Synthetic organic chemistry driven by artificial intelligence. *Nat. Rev. Chem.* **3**, 589–604 (2019).
75. Jorner, K., Brinck, T., Norrby, P.-O. & Buttar, D. Machine learning meets mechanistic modelling for accurate prediction of experimental activation energies. *Chem. Sci.* **12**, 1163–1175 (2021).
76. Jorner, K., Tomberg, A., Bauer, C., Sköld, C. & Norrby, P.-O. Organic reactivity from mechanism to machine learning. *Nat. Rev. Chem.* **5**, 240–255 (2021).
77. Zhang, J. L. et al. Towards single molecule switches. *Chem. Soc. Rev.* **44**, 2998–3022 (2015).
78. Irie, M., Fukaminato, T., Matsuda, K. & Kobatake, S. Photochromism of diarylethene molecules and crystals: memories, switches, and actuators. *Chem. Rev.* **114**, 12174–12277 (2014).
79. Bandara, H. M. D. & Burdette, S. C. Photoisomerization in different classes of azobenzene. *Chem. Soc. Rev.* **41**, 1809–1825 (2012).
80. Robertson, J. C., Coote, M. L. & Bissember, A. C. Synthetic applications of light, electricity, mechanical force and flow. *Nat. Rev. Chem.* **3**, 290–304 (2019).
81. Brongersma, M. L., Halas, N. J. & Nordlander, P. Plasmon-induced hot carrier science and technology. *Nat. Nanotechnol.* **10**, 25–34 (2015).
82. Anelli, P. L. et al. Molecular meccano. 1. [2]Rotaxanes and a [2]catenane made to order. *J. Am. Chem. Soc.* **114**, 193–218 (1992).
83. Jeppesen, J. O., Perkins, J., Becher, J. & Stoddart, J. F. Slow shuttling in an amphiphilic bistable [2]rotaxane incorporating a tetrathiafulvalene unit. *Angew. Chem. Int. Ed.* **40**, 1216–1221 (2001).
84. Heath, J. R. Molecular electronics. *Annu. Rev. Mater.* **39**, 1–23 (2009).
85. Coskun, A. et al. High hopes: can molecular electronics realise its potential? *Chem. Soc. Rev.* **41**, 4827–4859 (2012).
86. Chen, H. & Fraser Stoddart, J. From molecular to supramolecular electronics. *Nat. Rev. Mater.* **6**, 804–828 (2021).
87. Bruns, C. J. & Stoddart, J. F. *The Nature of the Mechanical Bond: From Molecules to Machines* (Wiley, 2016).
88. Zhou, C. et al. Revealing charge- and temperature-dependent movement dynamics and mechanism of individual molecular machines. *Small Methods* **3**, 1900464 (2019).
89. Chen, S. et al. Real-time observation of the dynamics of an individual rotaxane molecular shuttle using a single-molecule junction. *Chem* **8**, 243–252 (2022).
90. Yang, G. et al. Protonation tuning of quantum interference in azulene-type single-molecule junctions. *Chem. Sci.* **8**, 7505–7509 (2017).
91. Zhang, Y.-P. et al. Distinguishing diketopyrrolopyrrole isomers in single-molecule junctions via reversible stimuli-responsive quantum interference. *J. Am. Chem. Soc.* **140**, 6531–6535 (2018).
92. Cai, S. et al. Light-driven reversible intermolecular proton transfer at single-molecule junctions. *Angew. Chem. Int. Ed.* **58**, 3829–3833 (2019).
93. Li, J. et al. Direct measurement of single-molecule adenosine triphosphatase hydrolysis dynamics. *ACS Nano* **11**, 12789–12795 (2017).
94. Yang, Z. et al. Revealing conformational transition dynamics of photosynthetic proteins in single-molecule electrical circuits. *J. Phys. Chem. Lett.* **12**, 3853–3859 (2021).
95. He, G., Li, J., Ci, H., Qi, C. & Guo, X. Direct measurement of single-molecule DNA hybridization dynamics with single-base resolution. *Angew. Chem. Int. Ed.* **55**, 9036–9040 (2016).
96. He, G., Li, J., Qi, C. & Guo, X. Single nucleotide polymorphism genotyping in single-molecule electronic circuits. *Adv. Sci.* **4**, 1700158 (2017).
97. Marcus, R. A. Chemical and electrochemical electron-transfer theory. *Annu. Rev. Phys. Chem.* **15**, 155–196 (1964).
98. Skourtis, S. S., Waldeck, D. H. & Beratan, D. N. Fluctuations in biological and bioinspired electron-transfer reactions. *Annu. Rev. Phys. Chem.* **61**, 461–485 (2010).
99. Li, Y. et al. Mechanical stretching-induced electron-transfer reactions and conductance switching in single molecules. *J. Am. Chem. Soc.* **139**, 14699–14706 (2017).
100. Frisenda, R. et al. Stretching-induced conductance increase in a spin-crossover molecule. *Nano Lett.* **16**, 4733–4737 (2016).
101. Su, T. A., Li, H., Steigerwald, M. L., Venkataraman, L. & Nuckolls, C. Stereoelectronic switching in single-molecule junctions. *Nat. Chem.* **7**, 215–220 (2015).
102. Garcia-Manyes, S. & Beedle, A. E. M. Steering chemical reactions with force. *Nat. Rev. Chem.* **1**, 0083 (2017).
103. Walkey, M. C. et al. Chemically and mechanically controlled single-molecule switches using spiropyrans. *ACS Appl. Mater. Interfaces* **11**, 36886–36894 (2019).
104. Tamaki, T. et al. Mechanical switching of current–voltage characteristics in spiropyran single-molecule junctions. *Nanoscale* **12**, 7527–7531 (2020).
105. Aradhya, S. V. & Venkataraman, L. Single-molecule junctions beyond electronic transport. *Nat. Nanotechnol.* **8**, 399–410 (2013).
106. Mejía, L. & Franco, I. Force–conductance spectroscopy of a single-molecule reaction. *Chem. Sci.* **10**, 3249–3256 (2019).
107. Chen, H. et al. Interface engineering in organic field-effect transistors: principles, applications, and perspectives. *Chem. Rev.* **120**, 2879–2949 (2020).
108. Zhao, Y., Gobbi, M., Hueso, L. E. & Samorì, P. Molecular approach to engineer two-dimensional devices for CMOS and beyond-CMOS applications. *Chem. Rev.* **122**, 50–131 (2022).
109. Dulic, D. et al. One-way optoelectronic switching of photochromic molecules on gold. *Phys. Rev. Lett.* **91**, 207402 (2003).
110. Whalley, A. C., Steigerwald, M. L., Guo, X. & Nuckolls, C. Reversible switching in molecular electronic devices. *J. Am. Chem. Soc.* **129**, 12590–12591 (2007).
111. Katsonis, N. et al. Reversible conductance switching of single diarylethenes on a gold surface. *Adv. Mater.* **18**, 1397–1400 (2006).
112. Jia, C. et al. Covalently bonded single-molecule junctions with stable and reversible photoswitched conductivity. *Science* **352**, 1443–1445 (2016).
113. Jia, C. et al. Conductance switching and mechanisms in single-molecule junctions. *Angew. Chem. Int. Ed.* **52**, 8666–8670 (2013).
114. Chen, H. et al. Design of a photoactive hybrid bilayer dielectric for flexible nonvolatile organic memory transistors. *ACS Nano* **10**, 436–445 (2016).
115. Kim, Y. et al. Charge transport in azobenzene-based single-molecule junctions. *Phys. Rev. Lett.* **109**, 226801 (2012).
116. Cao, Y., Dong, S., Liu, S., Liu, Z. & Guo, X. Toward functional molecular devices based on graphene–molecule junctions. *Angew. Chem. Int. Ed.* **52**, 3906–3910 (2013).
117. Henzl, J., Mehlhorn, M., Gawronski, H., Rieder, K.-H. & Morgenstern, K. Reversible *cis–trans* isomerization of a single azobenzene molecule. *Angew. Chem. Int. Ed.* **45**, 603–606 (2006).
118. Choi, B.-Y. et al. Conformational molecular switch of the azobenzene molecule: a scanning tunneling microscopy study. *Phys. Rev. Lett.* **96**, 156106 (2006).
119. Alemani, M. et al. Electric field-induced isomerization of azobenzene by STM. *J. Am. Chem. Soc.* **128**, 14446–14447 (2006).
120. Meng, L. et al. Atomic force microscopy for molecular structure elucidation. *Angew. Chem. Int. Ed.* **60**, 12274–12278 (2021).
121. Li, H. B., Tebikachew, B. E., Wiberg, C., Moth-Poulsen, K. & Hihath, J. A memristive element based on an electrically controlled single-molecule reaction. *Angew. Chem. Int. Ed.* **59**, 11641–11646 (2020).
122. Fatayer, S. et al. Molecular structure elucidation with charge-state control. *Science* **365**, 142–145 (2019).
123. Dri, C., Peters, M. V., Schwarz, J., Hecht, S. & Grill, L. Spatial periodicity in molecular switching. *Nat. Nanotechnol.* **3**, 649–653 (2008).
124. Kazuma, E., Jung, J., Ueba, H., Trenary, M. & Kim, Y. Real-space and real-time observation of a plasmon-induced chemical reaction of a single molecule. *Science* **360**, 521–526 (2018).
125. Zhang, Q. et al. Photothermal effect, local field dependence, and charge carrier relaying species in plasmon-driven photocatalysis: a case study of aerobic nitrothiophenol coupling reaction. *J. Phys. Chem. C* **123**, 26695–26704 (2019).
126. Kazuma, E. & Kim, Y. Mechanistic studies of plasmon chemistry on metal catalysts. *Angew. Chem. Int. Ed.* **58**, 4800–4808 (2019).
127. Kazuma, E., Lee, M., Jung, J., Trenary, M. & Kim, Y. Single-molecule study of a plasmon-induced reaction for a strongly chemisorbed molecule. *Angew. Chem. Int. Ed.* **59**, 7960–7966 (2020).
128. Studer, A. & Curran, D. P. The electron is a catalyst. *Nat. Chem.* **6**, 765–773 (2014).
129. Hla, S.-W., Bartels, L., Meyer, G. & Rieder, K.-H. Inducing all steps of a chemical reaction with the scanning tunneling microscope tip: towards single molecule engineering. *Phys. Rev. Lett.* **85**, 2777–2780 (2000).
130. Shaik, S., Ramanan, R., Danovich, D. & Mandal, D. Structure and reactivity/selectivity control by oriented-external electric fields. *Chem. Soc. Rev.* **47**, 5125–5145 (2018).
131. Ciampi, S., Darwish, N., Aitken, H. M., Díez-Pérez, I. & Coote, M. L. Harnessing electrostatic catalysis in single molecule, electrochemical and chemical systems: a rapidly growing experimental tool box. *Chem. Soc. Rev.* **47**, 5146–5164 (2018).
132. Fahrenbach, A. C. et al. Solution-phase mechanistic study and solid-state structure of a tris(bipyridinium radical cation) inclusion complex. *J. Am. Chem. Soc.* **134**, 3061–3072 (2012).
133. Rempala, P., Kroulík, J. & King, B. T. A slippery slope: mechanistic analysis of the intramolecular Scholl reaction of hexaphenylbenzene. *J. Am. Chem. Soc.* **126**, 15002–15003 (2004).
134. Kim, Y., Komeda, T. & Kawai, M. Single-molecule reaction and characterization by vibrational excitation. *Phys. Rev. Lett.* **89**, 126104 (2002).
135. Stipe, B. C. et al. Single-molecule dissociation by tunneling electrons. *Phys. Rev. Lett.* **78**, 4410–4413 (1997).
136. Pan, S. et al. Design and control of electron transport properties of single molecules. *Proc. Natl Acad. Sci. USA* **106**, 15259–15263 (2009).
137. Liljeroth, P., Repp, J. & Meyer, G. Current-induced hydrogen tautomerization and conductance switching of naphthalocyanine molecules. *Science* **317**, 1203–1206 (2007).
138. Dujardin, G., Walkup, R. E. & Avouris, P. Dissociation of individual molecules with electrons from the tip of a scanning tunneling microscope. *Science* **255**, 1232–1235 (1992).
139. Martel, R., Avouris, P. & Lyo, I.-W. Molecularly adsorbed oxygen species on Si(111)-(7×7): STM-induced dissociative attachment studies. *Science* **272**, 385–388 (1996).
140. Shi, S.-H., Liang, Y. & Jiao, N. Electrochemical oxidation induced selective C–C bond cleavage. *Chem. Rev.* **121**, 485–505 (2021).
141. Sperry, J. B. & Wright, D. L. The application of cathodic reductions and anodic oxidations in the synthesis of complex molecules. *Chem. Soc. Rev.* **35**, 605–621 (2006).
142. Yoshida, J., Kataoka, K., Horcajada, R. & Nagaki, A. Modern strategies in electroorganic synthesis. *Chem. Rev.* **108**, 2265–2299 (2008).
143. Park, J. et al. Coulomb blockade and the Kondo effect in single-atom transistors. *Nature* **417**, 722–725 (2002).
144. Moth-Poulsen, K. & Bjørnholm, T. Molecular electronics with single molecules in solid-state devices. *Nat. Nanotechnol.* **4**, 551–556 (2009).
145. Hromadova, M. & Vavrek, F. Electrochemical electron transfer and its relation to charge transport in single molecule junctions. *Curr. Opin. Electrochem.* **19**, 63–70 (2020).

146. Nichols, R. J. Molecular electronics at electrode–electrolyte interfaces. *Curr. Opin. Electrochem.* **25**, 100650 (2021).
147. Perrin, M. L., Burzurí, E. & van der Zant, H. S. J. Single-molecule transistors. *Chem. Soc. Rev.* **44**, 902–919 (2015).
148. Bai, J., Li, X., Zhu, Z., Zheng, Y. & Hong, W. Single-molecule electrochemical transistors. *Adv. Mater.* **33**, 2005883 (2021).
149. Xu, B., Xiao, X., Yang, X., Zang, L. & Tao, N. Large gate modulation in the current of a room temperature single molecule transistor. *J. Am. Chem. Soc.* **127**, 2386–2387 (2005).
150. Díez-Pérez, I. et al. Ambipolar transport in an electrochemically gated single-molecule field-effect transistor. *ACS Nano* **6**, 7044–7052 (2012).
151. Li, Y. et al. Three-state single-molecule naphthalenediimide switch: integration of a pendant redox unit for conductance tuning. *Angew. Chem. Int. Ed.* **54**, 13586–13589 (2015).
152. Darwish, N. et al. Observation of electrochemically controlled quantum interference in a single anthraquinone-based norbornylogous bridge molecule. *Angew. Chem. Int. Ed.* **51**, 3203–3206 (2012).
153. Baghernejad, M. et al. Electrochemical control of single-molecule conductance by Fermi-level tuning and conjugation switching. *J. Am. Chem. Soc.* **136**, 17922–17925 (2014).
154. Haiss, W. et al. Redox state dependence of single molecule conductivity. *J. Am. Chem. Soc.* **125**, 15294–15295 (2003).
155. Pobelov, I. V., Li, Z. & Wandlowski, T. Electrolyte gating in redox-active tunneling junctions — an electrochemical STM approach. *J. Am. Chem. Soc.* **130**, 16045–16054 (2008).
156. Osorio, H. M. et al. Electrochemical single-molecule transistors with optimized gate coupling. *J. Am. Chem. Soc.* **137**, 14319–14328 (2015).
157. Leary, E. et al. Structure–property relationships in redox-gated single molecule junctions — a comparison of pyrrolo-tetrathiafulvalene and viologen redox groups. *J. Am. Chem. Soc.* **130**, 12204–12205 (2008).
158. Kay, N. J. et al. Single-molecule electrochemical gating in ionic liquids. *J. Am. Chem. Soc.* **134**, 16817–16826 (2012).
159. Li, Z. et al. Regulating a benzodifuran single molecule redox switch via electrochemical gating and optimization of molecule/electrode coupling. *J. Am. Chem. Soc.* **136**, 8867–8870 (2014).
160. Yin, X. et al. A reversible single-molecule switch based on activated antiaromaticity. *Sci. Adv.* **3**, eaao2615 (2017).
161. Ricci, A. M., Calvo, E. J., Martin, S. & Nichols, R. J. Electrochemical scanning tunneling spectroscopy of redox-active molecules bound by Au–C bonds. *J. Am. Chem. Soc.* **132**, 2494–2495 (2010).
162. Zhou, X.-S. et al. Do molecular conductances correlate with electrochemical rate constants? Experimental insights. *J. Am. Chem. Soc.* **133**, 7509–7516 (2011).
163. Lovat, G. et al. Room-temperature current blockade in atomically defined single-cluster junctions. *Nat. Nanotechnol.* **12**, 1050–1054 (2017).
164. Dickinson, E. J. F. & Wain, A. J. The Butler–Volmer equation in electrochemical theory: origins, value, and practical application. *J. Electroanal. Chem.* **872**, 114145 (2020).
165. Li, Y. et al. Transition from stochastic events to deterministic ensemble average in electron transfer reactions revealed by single-molecule conductance measurement. *Proc. Natl Acad. Sci. USA* **116**, 3407–3412 (2019).
166. Zhang, J. et al. Single-molecule electron transfer in electrochemical environments. *Chem. Rev.* **108**, 2737–2791 (2008).
167. Darwish, N. et al. Single molecular switches: electrochemical gating of a single anthraquinone-based norbornylogous bridge molecule. *J. Phys. Chem. C* **116**, 21093–21097 (2012).
168. Gross, L. et al. Atomic force microscopy for molecular structure elucidation. *Angew. Chem. Int. Ed.* **57**, 3888–3908 (2018).
169. Fatayer, S. et al. Reorganization energy upon charging a single molecule on an insulator measured by atomic force microscopy. *Nat. Nanotechnol.* **13**, 376–380 (2018).
170. Pavliček, N. et al. Synthesis and characterization of triangulene. *Nat. Nanotechnol.* **12**, 308–311 (2017).
171. Tan, S. et al. CO_2 dissociation activated through electron attachment on the reduced rutile TiO_2(110)-1×1 surface. *Phys. Rev. B* **84**, 155418 (2011).
172. Ulmer, U. et al. Fundamentals and applications of photocatalytic CO_2 methanation. *Nat. Commun.* **10**, 3169 (2019).
173. Tan, S. et al. Observation of photocatalytic dissociation of water on terminal Ti sites of TiO_2(110)-1×1 surface. *J. Am. Chem. Soc.* **134**, 9978–9985 (2012).
174. Zhu, X. et al. Vibration-assisted charge transport through positively charged dimer junctions. *Angew. Chem. Int. Ed.* **61**, e202210939 (2022).
175. Chen, H. et al. Electron-catalyzed dehydrogenation in a single-molecule junction. *J. Am. Chem. Soc.* **143**, 8476–8487 (2021).
176. Saveant, J. M. Catalysis of chemical reactions by electrodes. *Acc. Chem. Res.* **13**, 323–329 (1980).
177. Shaik, S. & Stuyver, T. *Effects of Electric Fields on Structure and Reactivity: New Horizons in Chemistry* (RSC Publishing, 2021).
178. Warshel, A. et al. Electrostatic basis for enzyme catalysis. *Chem. Rev.* **106**, 3210–3235 (2006).
179. Fried, S. D., Bagchi, S. & Boxer, S. G. Extreme electric fields power catalysis in the active site of ketosteroid isomerase. *Science* **346**, 1510–1514 (2014).
180. Welborn, V. V. & Head-Gordon, T. Fluctuations of electric fields in the active site of the enzyme ketosteroid isomerase. *J. Am. Chem. Soc.* **141**, 12487–12492 (2019).
181. Welborn, V. V., Ruiz Pestana, L. & Head-Gordon, T. Computational optimization of electric fields for better catalysis design. *Nat. Catal.* **1**, 649–655 (2018).
182. Liu, W. & Stoddart, J. F. Emergent behavior in nanoconfined molecular containers. *Chem* **7**, 919–947 (2021).
183. Morimoto, M. et al. Advances in supramolecular host-mediated reactivity. *Nat. Catal.* **3**, 969–984 (2020).
184. Grommet, A. B., Feller, M. & Klajn, R. Chemical reactivity under nanoconfinement. *Nat. Nanotechnol.* **15**, 256–271 (2020).
185. Kaphan, D. M., Toste, F. D., Bergman, R. G. & Raymond, K. N. Enabling new modes of reactivity via constrictive binding in a supramolecular-assembly-catalyzed aza-Prins cyclization. *J. Am. Chem. Soc.* **137**, 9202–9205 (2015).
186. Levin, M. D. et al. Scope and mechanism of cooperativity at the intersection of organometallic and supramolecular catalysis. *J. Am. Chem. Soc.* **138**, 9682–9693 (2016).
187. Zhang, L. et al. Electrochemical and electrostatic cleavage of alkoxyamines. *J. Am. Chem. Soc.* **140**, 766–774 (2018).
188. Gorin, C. F., Beh, E. S. & Kanan, M. W. An electric field–induced change in the selectivity of a metal oxide-catalyzed epoxide rearrangement. *J. Am. Chem. Soc.* **134**, 186–189 (2012).
189. Gorin, C. F., Beh, E. S., Bui, Q. M., Dick, G. R. & Kanan, M. W. Interfacial electric field effects on a carbene reaction catalyzed by Rh porphyrins. *J. Am. Chem. Soc.* **135**, 11257–11265 (2013).
190. Zang, Y. et al. Directing isomerization reactions of cumulenes with electric fields. *Nat. Commun.* **10**, 4482 (2019).
191. Stone, I. B. et al. Interfacial electric fields catalyze Ullmann coupling reactions on gold surfaces. *Chem. Sci.* **13**, 10798–10805 (2022).
192. Zhang, J., Coote, M. L. & Ciampi, S. Electrostatics and electrochemistry: mechanism and scope of charge-transfer reactions on the surface of tribocharged insulators. *J. Am. Chem. Soc.* **143**, 3019–3032 (2021).
193. Allen J. B. & Faulkner, L. R. *Electrochemical Methods: Fundamentals and Applications* 2nd Edn (Wiley, 2000).
194. Darwish, N. et al. Probing the effect of the solution environment around redox-active moieties using rigid anthraquinone terminated molecular rulers. *J. Am. Chem. Soc.* **134**, 18401–18409 (2012).
195. Eggers, P. K., Darwish, N., Paddon-Row, M. N. & Gooding, J. J. Surface-bound molecular rulers for probing the electrical double layer. *J. Am. Chem. Soc.* **134**, 7539–7544 (2012).
196. Wen, B.-Y. et al. Probing electric field distributions in the double layer of a single-crystal electrode with Angstrom spatial resolution using Raman spectroscopy. *J. Am. Chem. Soc.* **142**, 11698–11702 (2020).
197. Bhattacharyya, D. et al. Sub-nanometer mapping of the interfacial electric field profile using a vibrational stark shift ruler. *J. Am. Chem. Soc.* **144**, 14330–14338 (2022).
198. Zhang, L. et al. TEMPO monolayers on Si(100) electrodes: electrostatic effects by the electrolyte and semiconductor space-charge on the electroactivity of a persistent radical. *J. Am. Chem. Soc.* **138**, 9611–9619 (2016).
199. Capozzi, B. et al. Single-molecule diodes with high rectification ratios through environmental control. *Nat. Nanotechnol.* **10**, 522–527 (2015).
200. Hammett, L. P. The effect of structure upon the reactions of organic compounds. Benzene derivatives. *J. Am. Chem. Soc.* **59**, 96–103 (1937).
201. LeBlond, C. R., Andrews, A. T., Sun, Y. & Sowa, J. R. Activation of aryl chlorides for Suzuki cross-coupling by ligandless, heterogeneous palladium. *Org. Lett.* **3**, 1555–1557 (2001).
202. Heo, J. et al. Electro-inductive effect: electrodes as functional groups with tunable electronic properties. *Science* **370**, 214–219 (2020).
203. Sarkar, S., Patrow, J. G., Voegtle, M. J., Pennathur, A. K. & Dawlaty, J. M. Electrodes as polarizing functional groups: correlation between Hammett parameters and electrochemical polarization. *J. Phys. Chem. C* **123**, 4926–4937 (2019).
204. Vladyka, A. et al. In-situ formation of one-dimensional coordination polymers in molecular junctions. *Nat. Commun.* **10**, 262 (2019).
205. Cocker, T. L., Peller, D., Yu, P., Repp, J. & Huber, R. Tracking the ultrafast motion of a single molecule by femtosecond orbital imaging. *Nature* **539**, 263–267 (2016).
206. Marquardt, C. W. et al. Electroluminescence from a single nanotube–molecule–nanotube junction. *Nat. Nanotechnol.* **5**, 863–867 (2010).
207. Zhang, L. et al. Precise electrical gating of the single-molecule Mizoroki–Heck reaction. *Nat. Commun.* **13**, 4552 (2022).
208. Domulevicz, L., Jeong, H., Paul, N. K., Gomez-Diaz, J. S. & Hihath, J. Multidimensional characterization of single-molecule dynamics in a plasmonic nanocavity. *Angew. Chem. Int. Ed.* **60**, 16436–16441 (2021).
209. Ruggeri, F. S., Mannini, B., Schmid, R., Vendruscolo, M. & Knowles, T. P. J. Single molecule secondary structure determination of proteins through infrared absorption nanospectroscopy. *Nat. Commun.* **11**, 2945 (2020).
210. Du, S., Yoshida, K., Zhang, Y., Hamada, I. & Hirakawa, K. Terahertz dynamics of electron–vibron coupling in single molecules with tunable electrostatic potential. *Nat. Photon.* **12**, 608–612 (2018).
211. Zhan, C. et al. Single-molecule plasmonic optical trapping. *Matter* **3**, 1350–1360 (2020).
212. Aragonès, A. C. & Domke, K. F. Nearfield trapping increases lifetime of single-molecule junction by one order of magnitude. *Cell Rep. Phys. Sci.* **2**, 100389 (2021).
213. Paulus, B. C., Adelman, S. L., Jamula, Lindsey, L. & McCusker, J. K. Leveraging excited-state coherence for synthetic control of ultrafast dynamics. *Nature* **582**, 214–218 (2020).
214. Pavliček, N. & Gross, L. Generation, manipulation and characterization of molecules by atomic force microscopy. *Nat. Rev. Chem.* **1**, 0005 (2017).

215. Atobe, M., Tateno, H. & Matsumura, Y. Applications of flow microreactors in electrosynthetic processes. *Chem. Rev.* **118**, 4541–4572 (2018).
216. Pletcher, D., Green, R. A. & Brown, R. C. D. Flow electrolysis cells for the synthetic organic chemistry laboratory. *Chem. Rev.* **118**, 4573–4591 (2018).
217. Quek, S. et al. Mechanically controlled binary conductance switching of a single-molecule junction. *Nat. Nanotechnol.* **4**, 230–234 (2009).
218. Green, J. et al. A 160-kilobit molecular electronic memory patterned at 1011 bits per square centimetre. *Nature* **445**, 414–417 (2007).
219. Zhang, Y., Song, P., Fu, Q., Ruan, M. & Xu, W. Single-molecule chemical reaction reveals molecular reaction kinetics and dynamics. *Nat. Commun.* **5**, 4238 (2014).
220. Li, C.-Y. et al. Real-time detection of single-molecule reaction by plasmon-enhanced spectroscopy. *Sci. Adv.* **6**, eaba6012 (2020).
221. Treier, M. et al. Surface-assisted cyclodehydrogenation provides a synthetic route towards easily processable and chemically tailored nanographenes. *Nat. Chem.* **3**, 61–67 (2011).
222. Mishra, S. et al. On-surface synthesis of a nitrogen-embedded buckybowl with inverse Stone–Thrower–Wales topology. *Nat. Commun.* **9**, 1714 (2018).
223. Kazuma, E., Jung, J., Ueba, H., Trenary, M. & Kim, Y. Direct pathway to molecular photodissociation on metal surfaces using visible light. *J. Am. Chem. Soc.* **139**, 3115–3121 (2017).
224. Grill, L. et al. Nano-architectures by covalent assembly of molecular building blocks. *Nat. Nanotechnol.* **2**, 687–691 (2007).
225. Hammer, B. & Norskov, J. K. Why gold is the noblest of all the metals. *Nature* **376**, 238–240 (1995).
226. Wang, C., Chi, L., Ciesielski, A. & Samorì, P. Chemical synthesis at surfaces with atomic precision: taming complexity and perfection. *Angew. Chem. Int. Ed.* **58**, 18758–18775 (2019).
227. Goldsmith, B. R., Coroneus, J. G., Kane, A. A., Weiss, G. A. & Collins, P. G. Monitoring single-molecule reactivity on a carbon nanotube. *Nano Lett.* **8**, 189–194 (2008).
228. Choi, Y. et al. Single-molecule lysozyme dynamics monitored by an electronic circuit. *Science* **335**, 319–324 (2012).
229. Quílez-Pardo, J. Do the equilibrium constants have units? A discussion on how general chemistry textbooks calculate and report the equilibrium constants. *Int. J. Phys. Chem. Educ.* **11**, 73–83 (2019).
230. Sorgenfrei, S. et al. Label-free single-molecule detection of DNA-hybridization kinetics with a carbon nanotube field-effect transistor. *Nat. Nanotechnol.* **6**, 126–132 (2011).
231. Dutta Dubey, K., Stuyver, T., Kalita, S. & Shaik, S. Solvent organization and rate regulation of a Menshutkin reaction by oriented external electric fields are revealed by combined MD and QM/MM calculations. *J. Am. Chem. Soc.* **142**, 9955–9965 (2020).
232. Xu, L., Izgorodina, E. I., Coote, M. L. Ordered solvents and ionic liquids can be harnessed for electrostatic catalysis. *J. Am. Chem. Soc.* **142**, 12826–12833 (2020).

Acknowledgements
The authors thank Northwestern University for its continued support of this research. The research at Zhejiang University was supported by the Starry Night Science Fund of Zhejiang University Shanghai Institute for Advanced Study (grant number SN-ZJU-SIAS-006) and the National Natural Science Foundation of China (grant number 22273085). The research at Peking University was supported by the National Key R&D Program of China (grant numbers 2017YFA0204901, 2021YFA1200101 and 2021YFA1200102) and the National Natural Science Foundation of China (grant numbers 21727806, 21933001 and 22150013). X.G. acknowledges the Tencent Foundation through the XPLORER PRIZE and Frontiers Science Center for New Organic Matter at Nankai University (grant number 63181206). The authors also thank Shanghai ShengSheng Logistics for the financial support.

Author contributions
All authors contributed to the discussion of content, writing and editing of the manuscript prior to submission.

Competing interests
The authors declare no competing interests.

Additional information

Correspondence should be addressed to Hongliang Chen, Xuefeng Guo or J. Fraser Stoddart.

Peer review information *Nature Reviews Materials* thanks Thorben Cordes and the other, anonymous, reviewer(s) for their contribution to the peer review of this work.

Reprints and permissions information is available at www.nature.com/reprints.

Publisher's note Springer Nature remains neutral with regard to jurisdictional claims in published maps and institutional affiliations.

Springer Nature or its licensor (e.g. a society or other partner) holds exclusive rights to this article under a publishing agreement with the author(s) or other rightsholder(s); author self-archiving of the accepted manuscript version of this article is solely governed by the terms of such publishing agreement and applicable law.

© Springer Nature Limited 2022